PROBABILISTIC RISK ASSESSMENT AND THE PATH PLANNING OF SAFE TASK-AWARE AUTONOMOUS RESILIENT SYSTEMS (STAARS)

by

ULUHAN CEM KAYA

Presented to the Faculty of the Graduate School of

The University of Texas at Arlington in Partial Fulfillment

of the Requirements

for the Degree of

MASTER OF SCIENCE IN AEROSPACE ENGINEERING

THE UNIVERSITY OF TEXAS AT ARLINGTON

May 2019

To my family.

ACKNOWLEDGEMENTS

Starting from my thesis supervisors Dr. Atilla Dogan and Dr. Manfred Huber, I would like to express my deepest gratitude for those who directly or indirectly played an important role in my personal growth and academic career. I am grateful for their guidance and unconditional support throughout my education, and thankful for the opportunities and any resources that are provided to me at the University of Texas, Arlington. I would also like to state my special thanks to Dr. Manfred Huber for accepting me as his own student and believing in my success especially in those times that I couldn't. I learned a lot from his immense knowledge and colorful personality, and without him, I couldn't complete my research. I am sure that I will miss all those lab meetings and cheerful discussions we had, without forgetting Dr. Brian Huff's great contribution. Being around all of you taught me not just the necessary engineering skills, but also the importance of a great team and even more importantly having good persons in my life. I appreciate everything you added to me.

I cannot conclude without acknowledging my gratitude to the course professors, MAE department officials and my friends that helped me come so far. I owe a special thank to Dr. Onur Daskiran for being with me all along as my mentor and brother. Finally, for being the greatest team I've ever had, I would like to dedicate my degree to my family. All the sacrifices they have made for my future will not be forgotten.

May 8, 2019

ABSTRACT

PROBABILISTIC RISK ASSESSMENT AND THE PATH PLANNING OF SAFE TASK-AWARE AUTONOMOUS RESILIENT SYSTEMS (STAARS)

ULUHAN CEM KAYA, M.S

The University of Texas at Arlington, 2019

Supervising Professor: Dr. Atilla Dogan

Co-supervising Professor: Dr. Manfred Huber

Recent advancements on the unmanned systems manifest the potential of these technologies to impact our daily life. In particular, the unmanned aircraft systems (UAS) become ordinary for people in almost any area from aerial photography to emergency responses, from agricultural services to even autonomous deliveries. Increased autonomy and advancements in low-cost high-computing technologies made these compact autonomous solutions accessible to any party with ease. Easiness and affordability to access these systems accelerated the innovations and the novel ideas for the solution of diverse real-life problems. Despite its benefits, however, this widespread availability also resulted in the safety and regulatory concerns in general. In an autonomous flight task over a public space, besides the mission objectives and the benefits, concerns regarding the public safety, privacy, and the regulations have to be addressed systematically during the planning and considered in the decision-making process. Therefore, there is a need for a comprehensive framework that can

properly quantify and assess the risks incurred by the UAS operations to these concerns.

This thesis presents the development of a probabilistic risk assessment framework and a path planning implementation of a concept of Safe Task-Aware Autonomous Resilient Systems (STAARS) to address the safety concerns. STAARS is conceptualized to consider the safety by quantifying and assessing the risks, task-awareness by adapting different tasks and environments, and resiliency by withstanding and making decisions in adversarial conditions. As a result, a multi-objective decision-making capability is introduced in this concept.

The thesis aims to establish a framework that could be used for the path planning of UAS operations to quantify, assess and compare the risks incurred by these operations as well as the profits of the mission objectives such that a multi-objective optimization can be achieved with a task-level decision-making capability. The proposed framework consists of the risk assessment part where a probabilistic risk exposure concept and the UAS failure mode analysis are utilized and a generic utility-based approach for the multi-objective optimization part. In the next step, a commonly used path planning algorithm, which is rapidly-exploring random trees (RRT), is introduced. Finally, the implementation of the proposed framework for a couple of simple UAS scenarios are demonstrated using the path planner.

TABLE OF CONTENTS

ACKNOWLEDGEMENTS iv

ABSTRACT v

LIST OF ILLUSTRATIONS ix

LIST OF TABLES xi

Chapter Page

1. INTRODUCTION 1

1.1 Background and Motivation 1

1.2 Thesis Outline 3

2. PROBABILISTIC RISK ASSESSMENT FRAMEWORK 5

2.1 Risk Definition 5

2.1.1 Risks in UAS Operations 6

2.2 Related Work 8

2.2.1 Ground Safety Risk 9

2.2.2 Risk Assessment Frameworks 13

2.3 Proposed Risk Assessment Framework 15

2.3.1 Probabilistic Risk Exposure Map (PREM) 17

2.3.2 UAS Failure Modes and Ground Impact Distribution 22

2.3.3 Risk Function 27

3. PATH PLANNING ALGORITHMS 34

3.1 RRT Algorithms 35

3.1.1 RRT 36

3.1.2 RRT* 39

3.1.3 Bi-RRT* . . . 43
3.1.4 Multi-RRT* . . . 45
3.2 Heuristics . . . 48
3.2.1 Goal Bias . . . 48
3.2.2 Transition Test . . . 49
3.2.3 PREM Guided Sample Generation . . . 50
3.3 Path Optimization . . . 51
4. DERIVATION OF UTILITY (COST) FUNCTIONAL FOR THE PATH PLANNING OF STAARS OPERATIONS . . . 55
4.1 Path Utility Function . . . 56
4.2 Calculation of Point Utilities . . . 59
5. SIMULATION OF SIMPLE STAARS SCENARIOS . . . 62
5.1 Simulation Environment . . . 62
5.1.1 Implementation Details . . . 65
5.2 Scenarios . . . 70
5.2.1 Scenario 1 . . . 71
5.2.2 Scenario 2 . . . 76
6. CONCLUDING REMARKS AND FUTURE WORK . . . 82
6.1 Thesis Contribution . . . 82
6.2 Future Works . . . 83
REFERENCES . . . 85
BIOGRAPHICAL STATEMENT . . . 90

LIST OF ILLUSTRATIONS

Figure		Page
1.1	Three main concerns that are listed by FAA regarding UAS operations	2
2.1	Illustration of *frequency* and *severity* of a negative event on Risk Matrix	5
2.2	Risk considerations in UAS operations	7
2.3	Components of UAS ground risk models [1]	10
2.4	General risk assessment framework components[2]	14
2.5	Components of the proposed risk assessment framework	16
2.6	Construction of PREM from the data is represented in flowchart	18
2.7	An illustration of PREM construction by survey data and sensor update	23
2.8	Calculation of ground impact distributions is depicted in flow chart	24
2.9	Failure mode impact domains and combined ground impact probability distribution	28
2.10	Illustration of a failure event with $PREM$ and impact distribution (left) and the calculation of the risk of a point on the discritized failure area (right)	30
3.1	Illustration of simple RRT algorithm	38
3.2	Illustration of rewiring operation of RRT* algorithm	42
3.3	Illustration of the connection between trees in Bi-RRT* algorithm	45
3.4	Illustration of multi-tree RRT* algorithm	46
3.5	Illustration of PREM guided sample node generation	52
5.1	Failure mode impact domains and combined ground impact probability distribution	69

5.2 Case maps for Scenario 1 72
5.3 Results of the path planning for Scenario 1 - Case 1 73
5.4 Results of the path planning for Scenario 1 - Case 2 74
5.5 UAS package delivery map - Scenario 2 76
5.6 Results of the path planning for Scenario 2 - Case 1 78
5.7 Results of the path planning for Scenario 2 - Case 2 79

LIST OF TABLES

Table Page

5.1 Failure Mode Parameters 69

5.2 RRT Parameters for Simulations 70

5.3 Catastrophic Failure Event Rates for Scenario 2 80

CHAPTER 1

INTRODUCTION

1.1 Background and Motivation

Recent advancements on unmanned autonomous systems shape the way we think in almost every area. One of the most impacting and noticeable examples of these systems is the unmanned aircraft systems (UAS). Less than a decade, these systems have undergone a transformation which makes them common and easily reachable by any parties from being rare and mostly experimental. Technological developments on the electronics, battery systems, and the low-cost high-computing solutions had undeniable contributions to this trend. Various applications in civilian, commercial, and military fields have proven the usefulness of UAS technology and revealed its potential to impact our daily life and the future of numerous industries. However, despite the ease of access, high demand and potential, integration of UAS into the National Airspace System (NAS) has been relatively slow due to current restrictions on the UAS operations. Operating within NAS requires aircraft systems to have comprehensive certifications that ensure the satisfaction of rules and regulations set by the aviation authorities. Comparing the conventional and manned aircraft systems, current unmanned systems are lack of such documentation, and so, the reliability of these systems has not fully assessed yet. Therefore, UAS operations in the national airspace, especially over the populated areas, present a risk to people and property on the ground and the other airspace users. Certainly, this situation raises concerns, which are outlined by the FAA in [3] as:

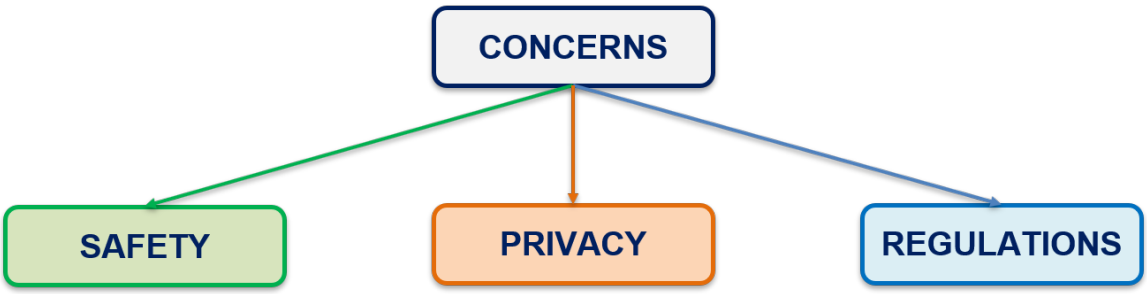

Figure 1.1: Three main concerns that are listed by FAA regarding UAS operations

According to the FAA, which is charged by the Congress in 2012 for the safe integration of UAS into NAS, these concerns are defined as the UAS collision with people and property both in the air and on the ground for the safety concerns, invasion of public privacy for the privacy concerns and a lack of rules and regulations that could address these concerns for the UAS operations. Lack of risk assessment tools, as we have for manned aircraft, unavailable historical data on the reliability of the used systems, and unclear privacy definition for the use of UAS technology form the basis for such concerns. In addition, current aviation regulations might be overly conservative or might not address the concerns for UAS operation, which limits benefiting from the full potential of UAS. Therefore, necessary tools and concepts should be developed, and the rules and regulations should be revised considering these concerns for the safe integration.

A recent study in [4] states that the importance of adopting the "risk-based" approach to the development of a regulatory framework for UAS operations has been lately recognized by the aviation authorities such as EASA and FAA, and it recommends the extension of current perspective on a quantitative risk assessment to look more holistically at the total safety risks. The essential argument in this study is that the application of currently used near-zero tolerance approach to the safety risk management process for UAS prevents the safety-beneficial operations. Instead, a

broader perspective to consider the net risk or benefit from these operations is suggested. Also, the current FAA approaches to the risk management are criticized for being based on qualitative and subjective risk analysis leading to the results that fail to be repeatable, predictable and transparent. On the other hand, the significance of establishing a quantitative framework to form the basis for the standards and decisions is underlined with the emphasize on the probabilistic risk analyses (PRAs).

In this thesis, the development of a comprehensive framework that can properly address the safety concerns by quantifying and assessing the risks incurred by the UAS operations as well as the benefits of these operations is introduced. The proposed framework includes a probabilistic risk assessment and a utility-based multi-objective optimization approach for the path planning of safe UAS operations using a concept of Safe Task-Aware Autonomous Resilient Systems (STAARS). STAARS is conceptualized to consider the safety by quantifying and assessing the risks, task-awareness by adapting different tasks and environments, and resiliency by withstanding and making decisions in adversarial conditions. As a result, a multi-objective decision-making capability is presented in this framework.

1.2 Thesis Outline

This thesis consists of mathematical modeling and the implementation of the concepts proposed for safe UAS operations. As the first step, components of the proposed probabilistic risk assessment framework is introduced, and the mathematical models of the components are formulated. In the second step, a path planning algorithm that will be used to implement the proposed framework is explained. In the third step, a more generic utility-based formulation is derived such that both the risks incurred by the UAS operations and the benefits (or objectives) of these operations can be considered within the same framework for a better decision process. Finally,

the developed models are implemented using the selected path planning algorithm to simulate simple UAS scenarios.

A brief overview of chapters is given below.

- ➔ **Chapter 2 - Probabilistic Risk Assessment Framework:** In this chapter, the risk considerations in UAS operations are explained, and the risk management approaches in Literature are outlined. After that, the proposed risk assessment approach is introduced in a framework by employing a probabilistic risk exposure concept and UAS failure mode analysis with ground impact distributions. Finally, a risk formulation for the risk assessment of the path planning process is derived from these concepts.
- ➔ **Chapter 3 - Path Planning Algorithms:** This chapter summarizes a family of path planning algorithms, which is the rapidly-exploring random trees (RRTs), that is used in this thesis to implement the proposed risk assessment concepts for simple UAS path planning scenarios. Pseudo-code of the algorithms and the heuristic approaches for the implementations are presented.
- ➔ **Chapter 4 - Derivation of Utility Functional for the Path Planning of STAARS Operations:** In this chapter, a multi-objective utility-based functional is derived to be used with the path planning algorithm as a cost function such that along with the risk considerations assessed by the proposed framework, the benefits of UAS operations can be integrated into the decision-making process for the path planning.
- ➔ **Chapter 5 - Simulation of Simple STAARS Scenarios:** This chapter describes the assumptions on the simulation environment and the implementation details for two different simple UAS path planning scenarios, and presents the results.

CHAPTER 2

PROBABILISTIC RISK ASSESSMENT FRAMEWORK

2.1 Risk Definition

The word "Risk" is used in numerous distinct fields from economy to health sector, to various social areas, to engineering disciplines, and it has a number of definitions and interpretations. In general, the risk is associated with the possibility of a negative event such as harm, loss, accident or disaster, where the qualitative and/or quantitative terms are used to interpret the consequences of the associated risk. One of the most common interpretations of the risk is made by using two terms: the *frequency* (probability) of the occurrence of the negative event and the *severity* (or consequence) of this negative event. To illustrate, the frequency and the severity categories of a risk scenario is shown with qualitative measures in Figure 2.1, which this table is also known as the risk matrix, [2].

Likelihood	Severity				
	Negligible	**Minor**	**Moderate**	**Critical**	**Catastrophic**
Unlikely	LOW	LOW	MEDIUM	MEDIUM	HIGH
Rare	LOW	LOW	MEDIUM	HIGH	HIGH
Occasional	LOW	MEDIUM	MEDIUM	HIGH	EXTREME
Likely	MEDIUM	MEDIUM	HIGH	EXTREME	EXTREME
Definite	MEDIUM	HIGH	HIGH	EXTREME	EXTREME

Figure 2.1: Illustration of *frequency* and *severity* of a negative event on Risk Matrix

where it is also common to represent these categories in measurable units such as the occurrence frequency ranges and the cost of possible loss or the fatalities.

There are two approaches to the risk concept: deterministic and probabilistic risks [5]. Deterministic approaches focus on the impact of a single risk event where the inputs of the risk model are known, and the outcomes can be observed. On the other hand, the probabilistic risk considerations include all possible events, their likelihood, and associated impacts, and they can account for the uncertainties on the hazardous events and incomplete knowledge of underlying phenomena. Although the number of factors to be accounted for and the other drivers that affect the stationarity of the risk can make the probabilistic risk assessments a challenging task, these assessments provide more comprehensive solutions for the potential risk conditions and can guide the decision process with a higher level of confidence. As a result, probabilistic risk assessment approaches get more and more attention and increasingly become the standard for risk management applications.

2.1.1 Risks in UAS Operations

Dynamics of the operating environment, complex vehicle systems, and many other contributing factors make UAS operations inherently the subject of the risk assessment. In this work, the risk is defined to be the negative condition that is resulted from the operation of a UAS; therefore, the risks to the success of a UAS mission are intentionally excluded. The literature search revealed that the risk considerations are grouped under three main categories; safety, privacy, and environmental impacts as tabulated in Figure 2.2.

Among these categories, safety concerns attract the most attention since it has a direct impact on the society, and they should be addressed primarily before any safety critical operation. Insufficient empirical data on the UAS reliability and outcome of

RISK CONSIDERATIONS		DESCRIPTION	OUTCOMES
SAFETY	Ground Risk	Collision with terrain or objects on the ground Damage to people/property on the ground	Injury or Fatality Damage to Property Impact on Society
	Air-to-Air Risk	Mid-air collisions with another UAS or manned aircrafts Damage to people/property on the air	
PRIVACY		Violations of public, organizational or indivudal privacies Tresspassing "No-Fly-Over" zones	Impact on Society
ENVIRONMENTAL		Environmental hazards resulted from possible UAS impacts Bush fires, chemical conteminant released, etc.	Impact on Environment

Figure 2.2: Risk considerations in UAS operations

the failures is the primary source of these safety concerns. In fact, to gain public trust in these technologies, establishing strong comprehensive rules and regulations in safety management procedures is an essential requirement. On the other hand, despite the non-negligible significance of the other categories, due to the relatively less impact on people's daily life, less attention is paid on privacy and environmental risks. Moreover, the lack of well-defined privacy terms and conditions for the UAS operations makes addressing the privacy concerns a non-trivial task, [6]. It is also possible to assume that minimizing the environmental impacts can be achieved by protective designs, preventive actions and the other similar methods, and comparing the safety risks, environmental risk considerations can be eliminated to the insignificant levels.

Safety risks posed by UAS operations are classified in two subcategories as ground risks and air-to-air risks. UAS ground risks occur in the event of a collision with terrain or the objects on the ground and result in damage to the people and/or properties on the ground. Whereas, air-to-air risk condition represents the collision with the other airspace users such as manned aircraft or another UAS, and potential damage to the people and/or property in the air. It is worth mentioning that air-to-air type risks also have the secondary effects on the ground in the form of falling debris impacts. However, the majority of the work is done in the ground safety risk considerations comparing to air-to-air risks due to the relatively highest impact on the

people's daily life and it is more likely to occur. The main reason for the higher occurrence likelihood is the current regulations that limit the UAS operations in visual line of sight (VLOS) and under 400 feet altitude. In addition, air-to-air collisions between most of the manned aircraft and the current commercially available UAS platforms are predicted to be insignificant for these platforms due to their incomparable sizes.

Privacy risks can be summarized as the violation of privacy rights of individuals, organizations, or public domain without involving controversial discussions, [7]. These risks stem from the way that UAS missions are carried out, rather than the operation itself. The instrumentation on the UAS platforms and the other technological capabilities used in data collection such as image, video or voice recording in high qualities raise a public concern regarding the possible abuse of the collected data or even the data collection itself without explicit permission.

In the last category, the environmental impacts of UAS operations are considered. These impacts are associated with the hazardous events that influence specifically the environmental condition in the form of chemical contamination, fire hazard, disturbance of the wildlife, and the other possible outcomes, [8, 9].

Objective of the risk assessment for UAS operations is to quantify identified risk conditions, and if possible, to keep them under an acceptable level.

2.2 Related Work

In literature, there are a number of studies on the risk analysis of UAS operations, where the majority of the work is done on the safety aspect of the risk considerations, in particular, the ground safety risks, due to the outlined reasons in the previous section. In these works, various approaches have been made on the estimation of ground collision risks posed by the UAS to people and properties on the ground. Several studies focus on the identification of possible UAS mishaps and

the estimation of the ground impacts by incorporating the detailed failure analysis, and there are also fewer studies attempting to develop a comprehensive risk assessment framework to address the ground safety concerns. The following sections will summarize some of the works mentioned here.

2.2.1 Ground Safety Risk

Ground safety term in the scope of the risk assessment of UAS operations is used to refer the impact of a UAS platform to the terrain or ground objects such as people, buildings or the other properties on the ground. As a result, consideration of the ground risks is particularly significant for the UAS operations over the populated (urban) areas and the regulation authorities who wish to establish complementary risk management systems.

In [1], Washington et al. partition the ground risk as to the primary and secondary hazards. The primary hazard is defined to be the direct impact of the UAS platform or its parts with the ground, and the secondary effects of the impact are exemplified as the spread of fires, vehicle accidents, the collapse of buildings, or release of hazardous materials affecting people and properties on the ground. Their study is based on a comprehensive review of the existing ground risk models, although none of the secondary hazards are addressed in these models. Figure 2.3, cited from their work, is a good representation of the general components of a ground risk model for UAS.

As can be seen from the diagram, components are divided into two groups according to their point of view to the ground risk. The first group investigates the effect of the platform and its operational conditions on the contribution of ground risk, whereas, the second group focuses on modeling the effect of exposed entities on

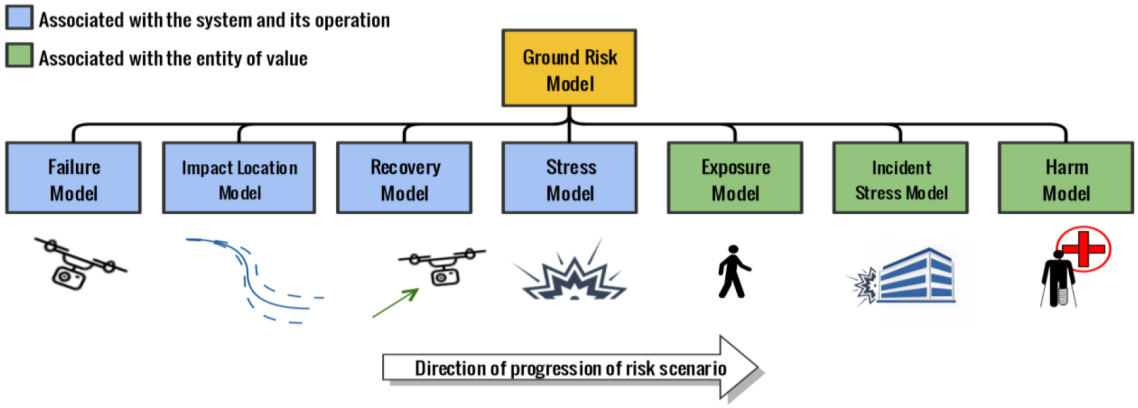

Figure 2.3: Components of UAS ground risk models [1]

the risk factors. There are valuable studies for each of these components. However, only the subset of these studies and components will be outlined here.

UAS failure models aim to capture the underlying factors contributing to the occurrence of failure modes and the uncertainty associated with the process. These factors include the system configuration, environmental conditions, and any other potential factors that can lead the UAS platform to a ground impact. One of the most practiced techniques is Failure Mode Effect Analysis (FMEA) that is widely used in system reliability assessments. FMEA technique first divides the system into more manageable subsystems, then, for each subsystem, possible failure modes, their propagation characteristics and probabilistic models to represent the occurrence of failure modes are identified. [10] performs FMEA by conducting a series of flight test experiments using various sUAS platforms including fixed-wing aircraft and multi-rotor platforms under off-nominal conditions. The effects of the rotor failures, the control surface servo failures, loss of GPS, and degraded IMU sensor readings are tested in their flight scenarios. Another important work on the identification of possible failure modes is carried out by Belcastro et al. in [11] over an extensive data set about UAS mishaps with more than hundred reports collected from a variety of

sources including government accident reports and media reports. In their research, they accomplish a detailed categorization of the mishap precursors and individual contributions of these identified hazards. Significance of subdividing and analyzing individual components of a system is to be able to understand and distinguish the behavior of each subsystem so that under off-nominal conditions, the behavior of the whole system can be predicted. It is also important to note that even though some of these analyses include the evaluation of multiple subsystem reactions, the effect of chain relation between subsystems needs further attention.

The impact location models, given a failure condition, try to predict the possible UAS impact position and the affected zone on the ground. Predictions are made using two different approaches with deterministic and probabilistic models. Deterministic models implement model-based designs and deterministic equations to obtain impact locations by specifying all the initial conditions and parameters neglecting the uncertainties. On the other hand, probabilistic approaches can also account for the effects of uncertainties on the prediction of final impact locations by introducing stochastic and random processes for the representation of the system, operational conditions or environmental factors. Considering the dynamics of the operating conditions and many other unknown factors that could affect the vehicle states, the latter approach gives a more promising future to model the real-life scenarios. Furthermore, the literature has several other areas, mainly focusing on these predictions. To name a few, safety range calculations for the launch vehicles, atmospheric re-entry and ballistic trajectory calculations are closely related to the problem defined under UAS impact location predictions.

In [12], flight computer failure and resulting frozen control surfaces condition are studied to predict the potential ground impact locations of a fixed-wing UAV. Their prediction method based on the average glide angle of the aircraft during the

failure descent until the crash happens. Although they use a deterministic model of the aircraft, introducing Monte Carlo simulations with randomized failure times, a probabilistic representation of the ground impact location is obtained. It is worth mentioning here that the characteristics of impact locations heavily depend on the failure modes as well as the type of aircraft itself. Ball et al. in [13] formulate various ground impact models for both rotary and fixed-wing type aircraft including several different failure flight regimes such as diving, gliding or auto-rotation, and their potential collision scenarios. Also, their lethal kinetic energy approach to finding the lethal area affected by the UAS impact is particularly important to for the ground risk assessment. Another valuable work is presented in [14] where the probability distribution of ground impact points for small UASs at ballistic descent is obtained in closed form. Cour-Harbo embeds the second order drag model in his probabilistic approach, and the effect of varying wind conditions is represented in his ground impact distribution.

The exposure models investigate the temporal and spatial dependencies of the third-party risk exposures on the ground. Third-parties are defined in the context of aviation risk management to be the people and properties not associated with, nor deriving any direct benefit from the operation of UAS, and their exposures to the risk are the primary concern by the aviation regulations. There are various models developed to address and quantify the ground exposures. Some of the most commonly used models utilize simple spatial distributions such as uniform exposure models to express exposure characteristics. In these models, spatial and temporal variations of the actual exposure are often neglected, and so, their approximations are only valid for relatively static and simple exposure distributions. On the other hand, there are also more comprehensive models introduced to address the dynamic and geospatially varying exposures. For example, a model developed by Melnyk in his doctoral stud-

ies, [15], considers the population distribution to integrate the temporal variation of exposure according to a study, in [16], on how and where people spend their time. There are numerous factors affecting the exposure characteristics on the ground, such as population behavior, uncertainty on the geospatial data, and potentially many others. Therefore, for more realistic modeling of the actual underlying exposures, predictive and dynamic analysis should also be incorporated with the current approaches.

2.2.2 Risk Assessment Frameworks

Several studies have tackled the problem of establishing a systematic framework for the assessment of risks incurred by the UAS operations. One of the most detailed work has been put forward by Melnyk in [15]. In his work, he provides a framework to address and predict UAS safety by analyzing several reliability and safety levels and employing casualty expectation method to quantify the risk of UAS operations. He uses event tree structure to represent the failure events with varying parameters that affect the occurrence or outcome of the events in the quantification of the risk, and he integrates a large number of factors impacting risk assessment such as ground exposure characteristics, various properties of UAS platforms, operating environment and many other contributing factors by successfully reviewing the previous works. More importantly, he describes how the framework could be used to assist the safe UAS integration which is proposed as utilizing the target level of safety (TLS) concept in the form of failure frequency rates to compare the evaluated risks with the acceptable limits.

Clothier has introduced another similar work in [17], which neatly summarizes the safety risk management process in a framework for the UAS operations. Acceptable level of safety concept has also been followed in his study with a higher level

approach. Some of the reviews and explanations about the common risk identification and analysis tools are particularly useful in this paper for the development of a general risk assessment framework.

Some other studies in this very topic have been conducted in [19, 18, 2], which also forms the starting point of the proposed risk assessment framework in this thesis. An agent-based modeling and simulation approach for the safety evaluation framework using modular construction of safety analysis metric introduced in [19], a probabilistic model-based approach and an effort to develop a real-time quantitative risk assessment framework employing casualty expectation and UAS ground impact prediction models in [18] and [2] are quite valuable resources one should have definitely reviewed before working on the development of a new risk assessment concept.

Figure 2.4 represents the general risk assessment diagram, cited from [2].

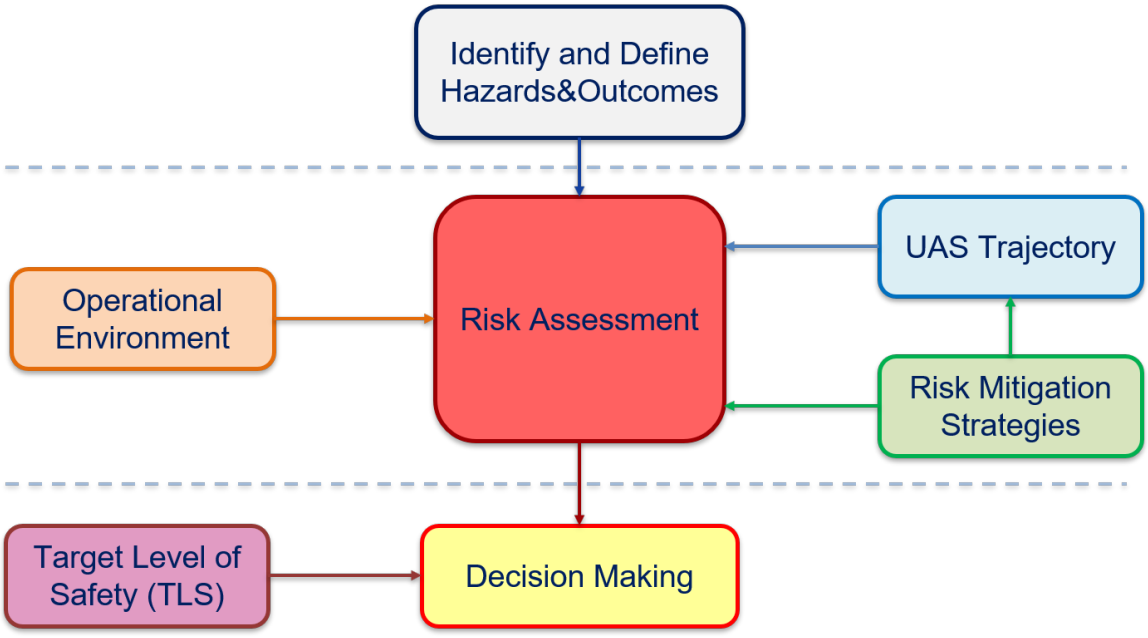

Figure 2.4: General risk assessment framework components[2]

According to this diagram, risk assessment has three stages. In the first stage, the hazards (negative events) and their outcomes are identified and defined. In the second stage, considering the operational environment and the risk mitigation strategies, assessment of the risk along the UAS trajectory is carried out. Finally, in the third step, the decision is made comparing the target level of safety with the assessed risk values. Generic information flow represented in this diagram will largely be adopted during the development of a risk assessment framework proposed in this thesis. However, the TLS approach, which is used in some of the previous works, will not be integrated with the proposed framework since its applicability to the UAS operations is not validated nor predicted to be feasible. In addition, the mitigation strategies to reduce the risk conditions are intentionally left outside of this work.

2.3 Proposed Risk Assessment Framework

Considering the literature search on the risk analysis of UAS operations, findings reveal that Equivalent Level of Safety (ELOS) or Target Level of Safety (TLS) approaches in risk assessment and decision-making processes are not straightforward for the operations related to UAS. The main reason is basically the way that the safety considerations are done. ELOS and TLS approaches establish a systematic way of describing required minimum safety conditions to satisfy, and they inform the decision-making process by constructing the ground rules. However, since these approaches are principally developed for the manned flight operations, their safety considerations are inherently based on the safety of the first-party which directly involves with the flight operations such as passengers, flight crews and ground teams. Therefore, the applicability of such concepts to UAS operations, where the safety of the third-parties is rather considered, is not possible in their current form. Instead, a risk assessment framework is proposed in this thesis to assess the ground safety

risks exposed by UAS operations. The proposed framework can also be utilized to establish the level of safety approaches along with further detailed analysis and it can be used as a decision support tool.

The proposed risk assessment framework has a similar structure with the general risk assessment framework depicted in Figure 2.4. It consists of three stages; the first stage employs the risk exposure model and UAS failure model with ground impact analysis to identify and define the possible risks and their outcomes, the second stage implements a path planning algorithm to find the paths for the UAS mission considering the operational environment and the risk assessment considerations over the trajectories, and finally, the third stage is the decision-making step which compares the found paths according to their risk conditions to find the least risky path for the mission. Components of the proposed framework are illustrated in Figure 2.5.

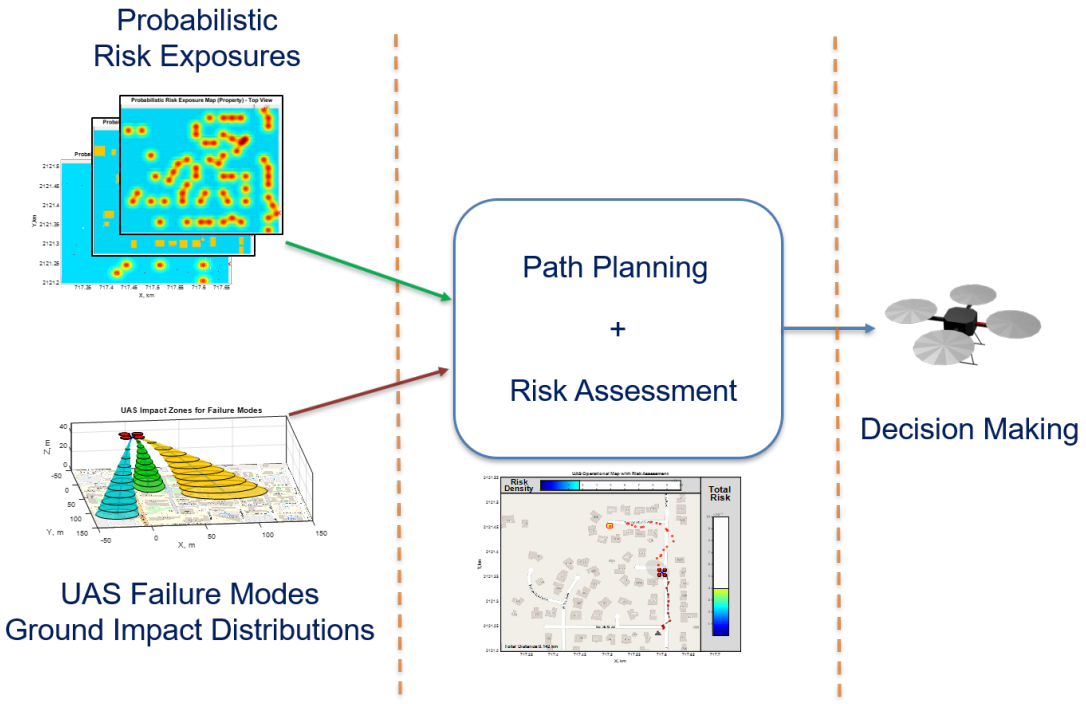

Figure 2.5: Components of the proposed risk assessment framework

Revisiting Figure 2.3, it can be seen that the proposed approach includes failure model, impact location model, and exposure model subcategories during the ground risk assessment. The rest of the models are currently excluded from the framework, but, for a more comprehensive and realistic representation of the actual risk conditions, these features can be added to the current framework.

In below sections, probabilistic risk exposure map (PREM) concept, modeling of UAS ground impact location distribution and the risk function to be used in the risk assessment of the path planning process are introduced and explained, respectively.

2.3.1 Probabilistic Risk Exposure Map (PREM)

Probabilistic risk exposure map (PREM) concept is used to model the risk of exposure on the ground to the presence of UAS in the air with a distribution where it is represented as a function of time and position on the ground. To illustrate a risk exposure distribution over a populated area, considering the population scattered on the ground, the higher the population in a specific area subjected to UAS operation is, the higher the risk of exposure (such as being hit by UAS or privacy violation) will be observed over that area, whereas, the areas with lower population will potentially have less risk exposure due to operations. Basically, PREM relates the spatial and temporal distributions of the ground objects that are considered in the safety evaluation to a distribution map, which later on, it will be used in the risk assessment along with UAS failure and ground impact models.

In this concept, the operation of UAS in urban/suburban areas is treated as a risk to the safety of bystanders, properties, and the other ground objects. Moreover, privacy and regulatory concerns regarding these operations can be addressed within the same concept. Thus, multiple objectives can be achieved by the PREM which consists of multiple layers corresponding to different types of risk classifications such

as the risk of flying over people (or traffic), of flying closely over residential units, or of violating restricted airspace. The flexibility of the concept also allows fusing various risk layers into the same risk map. The advantage of having only one map is that once all the risk types are fused and included in the PREM, decision-making strategies do not need to distinguish between different types of risks since the map already contains the required information.

The construction of PREM can be achieved by using various data sources. Figure 2.6 depicts the flowchart of PREM construction from different categories that are used to collect data from.

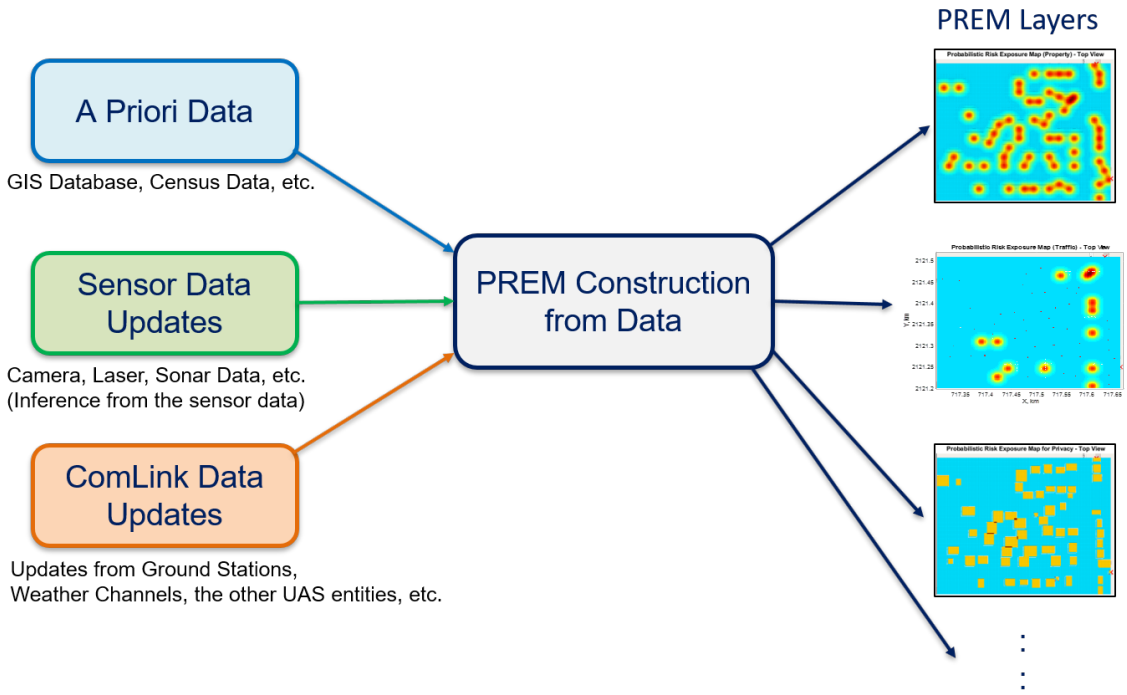

Figure 2.6: Construction of PREM from the data is represented in flowchart

According to Figure 2.6, data sources are divided into three categories. In the first category, data is received in the form of a priori data such as available geograph-

ical information database, census or survey mapping data, etc. This type of data source, which potentially consists of large data sets, can be accessed and efficiently utilized in accordance with the UAS operational plan. Therefore, this step refers to "offline planning" phase before the mission starts. The second and third categories refer to "online planning" phase of the UAS mission. In these categories, data required for the construction of risk exposures are obtained in the form of data updates from the vehicle's own sensors and through a communication link. Depending on the capabilities and the risk assessment considerations, various sensors or communication resources can be employed to construct, verify, and modify PREM layers. It is also worth noting that the "data" term used in this concept does not refer to raw data, instead, the usable information is meant by data.

Before the formulation of PREM construction, a few assumptions are made to simplify dealing with continuous space and distributions. First, assume that a risk layer is formed by the contribution of the individual risk exposure sources of the same type, $\{S_1, S_2, ..., S_N\}$, where they are independently modeled and discretely placed across the map. Also, assume that these individual sources and their distributions are given by a mapping data source M with the current information $e(t)$. Under these assumptions, risk exposure at a particular location and time can be characterized by two factors, namely **i)** the probability density of the risk exposure condition R at a location x and time t given the mapping M and an individual exposure source S_j, $p(R(x,t)|M(e(t)), S(t) = S_j)$, and **ii)** the probability of given individual exposure source S_j to capture total underlying risk exposure condition given M, $P(S(t) = S_j|M(e(t))$. Basically, the first term represents the spatial and temporal distribution of the risk exposure caused by the given source as a probability density function, while the second term models how much individual source S_j contributes to total risk

exposure. By the product of these two factors, the probability distribution of the i^{th} layer of the risk exposure for the given information can be constructed as

$$p(R^i(x,t)|M^i(e(t))) = \sum_{j=1}^{N} \Big[p(R^i(x,t)|M^i(e(t)), S^i(t) = S^i_j)\Big] \Big[P(S^i(t) = S^i_j|M^i(e(t)))\Big] \tag{2.1}$$

where N is the total number of discrete risk exposure sources. This formulation can be also thought as the weighted sum of distributions or the mixture of distributions.

In addition, assuming that mapping information about the underlying risk exposures is received from the discrete mapping sources, $M_{1,2,3,...}$, such as satellite maps, camera images, lidar maps or any other sources, conditioning on $M(e(t))$ in Equation (2.1) can be eliminated by introducing a probability term in Equation (2.2) to quantify the reliability of the data received from the mapping source M for the current information. This term models the uncertainty on the data collection during the PREM construction and it can be referred to the situational-awareness of the system. By this approach, a priori knowledge about the environment and the risk conditions can be updated as the new information gained, or the evidence collected, by any means.

$$PREM^i: \quad p(R^i(x,t)) = \sum_{M \in \{M_1, M_2, ..\}} \Big[p(R^i(x,t)|M^i(e(t)))\Big] \Big[P(M^i(e(t)))\Big] \tag{2.2}$$

Note that Equations (2.1) and (2.2) are generic equations to model PREM. However, for the simulations carried out in this thesis, the time dependency of the underlying process, and the uncertainty on the risk exposure mapping sources are intentionally excluded. Therefore, the underlying risk exposure is assumed to be stationary, and uncertainty on the mapping is neglected ($P(M(e) = APriori) = 1$). A new formulation of the ith layer of PREM becomes:

$$PREM^i: \quad p(R^i(x)) = \sum_{j=1}^{N} p(R^i(x)|S^i = S^i_j(l_j, m_j))P(S^i = S^i_j(l_j, m_j)) \tag{2.3}$$

where l_j is the center location of the individual risk exposure source, and m_j is the modeling parameter of the risk exposure distribution for this source. Each source is identified by these two parameters. This approach gives us the flexibility to model the total risk exposure distribution as a mixture of distributions over the discrete set of locations.

Furthermore, multiple PREM layers can be integrated into the same map in this approach by assigning weight factors for each layer according to their importance. However, it is important to note that, the accumulation of different risk types over a trajectory might differ from each other. One clear example is that while the privacy risks might be purely depending on the current location of the UAS and accumulated over time, UAS platform impact related risks would require where the platform failed and what the state of the vehicle was at the failure as well. Therefore, one should differentiate the dissimilar risk types during fusing. Nevertheless, one risk map fusing all the similar risk types (layers) can be formulated as below

$$p(R(x)) = \sum_{i \in \{a,b,\ldots\}} w^i p(R^i(x)) \quad \text{or} \quad PREM = \sum_{i \in \{a,b,\ldots\}} w^i PREM^i \tag{2.4}$$

where w^i is the weighting of the risk type i with the condition of $\forall i : w^i \geq 0, \sum_i w^i = 1$.

Another advantage of fusing multiple risk types in this approach is that every UAS mission may impose a different set of weights on various risk conditions. For instance, a weight on the privacy risk of residences would differ widely from a UAS executing the task of pizza delivery to transferring a medicine task. By this approach, only changing weights w^i in Equation (2.4), task-awareness of the system can be achieved, even during task execution. On the other hand, one might argue that the

risk exposure should not differ from one mission to another mission; instead, it should stay the same if nothing has changed on the ground. This argument might actually have a point to some extent. Hence, the task-awareness of the system will be revisited in Chapter 4 by a new approach using utility-based UAS mission planning.

An illustration of the PREM construction is depicted in Figure 2.7. A region consisting of discrete rectangular areas denoted with campus, forest, park and residential areas are selected for a UAS operation shown in Figure 2.7(a).

Figure 2.7(b) illustrates how the consensus or survey data about the population statistics for the different categories of regions are used to construct a PREM layer. Survey data is usually given as average values such as a hundred people per square mile, and here, it is used to lay down uniform distributions on the corresponding areas to model the risk of exposure. Usage of this information for the illustrative purpose is depicted for the streets, distinct areas, and building blocks. This type of PREM construction, as mentioned before, can be obtained using a priori data sources in the offline phase of the mission planning.

In addition, a simple scenario of PREM construction from sensor updates is illustrated in Figure 2.7(c). In this scenario, a group of people and traffic vehicles inside the sensor range of UAS platform are detected, and the distribution of the risk exposures are assigned on them as well. This simple scenario basically depicts how PREM is constructed during the online phase of the UAS mission. The similar examples can be populated using the other data sources such as communication link between the ground station and UAS or information from the other UASs.

2.3.2 UAS Failure Modes and Ground Impact Distribution

In this section, ground impact modeling of the UAS platform due to failure modes are investigated briefly, and a generic formulation is derived as an impact

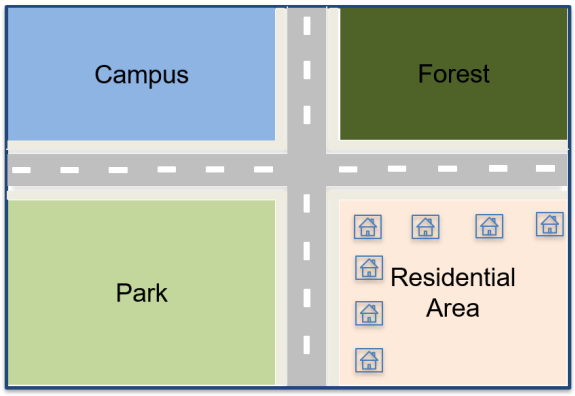

(a) An illustrative map of the region for UAS operation

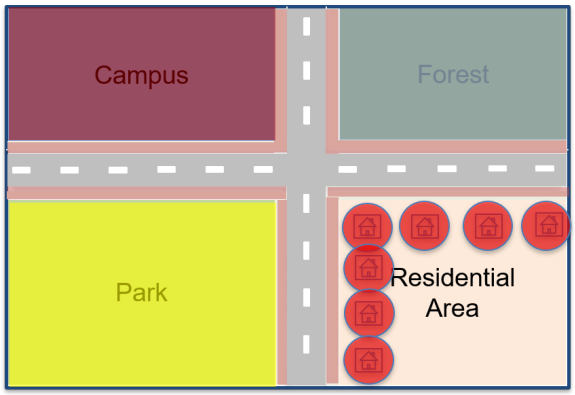

(b) A simple construction of PREM from a consensus/survey data

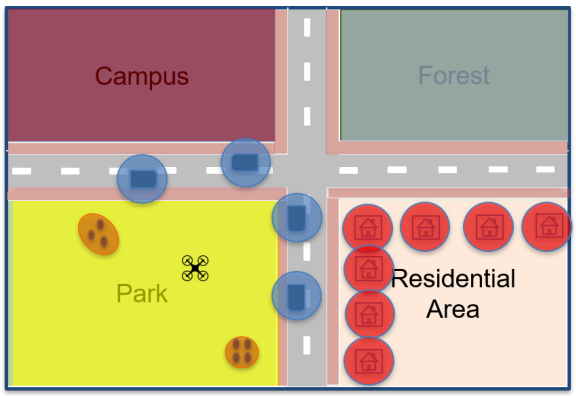

(c) A simple construction of PREM from sensor updates

Figure 2.7: An illustration of PREM construction by survey data and sensor update

probability distribution on the ground. Modeling the actual behavior of an unmanned aircraft system under critical failure conditions is not trivial due to the inherent nature of the operating environment and non-linearity of vehicle dynamics. There is a considerable amount of work done on this specific topic to identify the possible behaviors and to assess the reliability of these systems. As with the fault tree analysis, [20], failure mode analysis (FMEA) is one of the common methods to model the resulting behavior of the system under certain failure conditions, which are called failure modes, [10, 11]. In FMEA method, first, possible failure conditions are identified under distinct categories according to their root cause, and a detailed investigation is carried out to determine the occurrence rates and possible outcomes of the individual failure modes. In this thesis, UAS impact location on the ground is modeled using FMEA framework. Figure 2.8 shows the flowchart to obtain ground impact distributions.

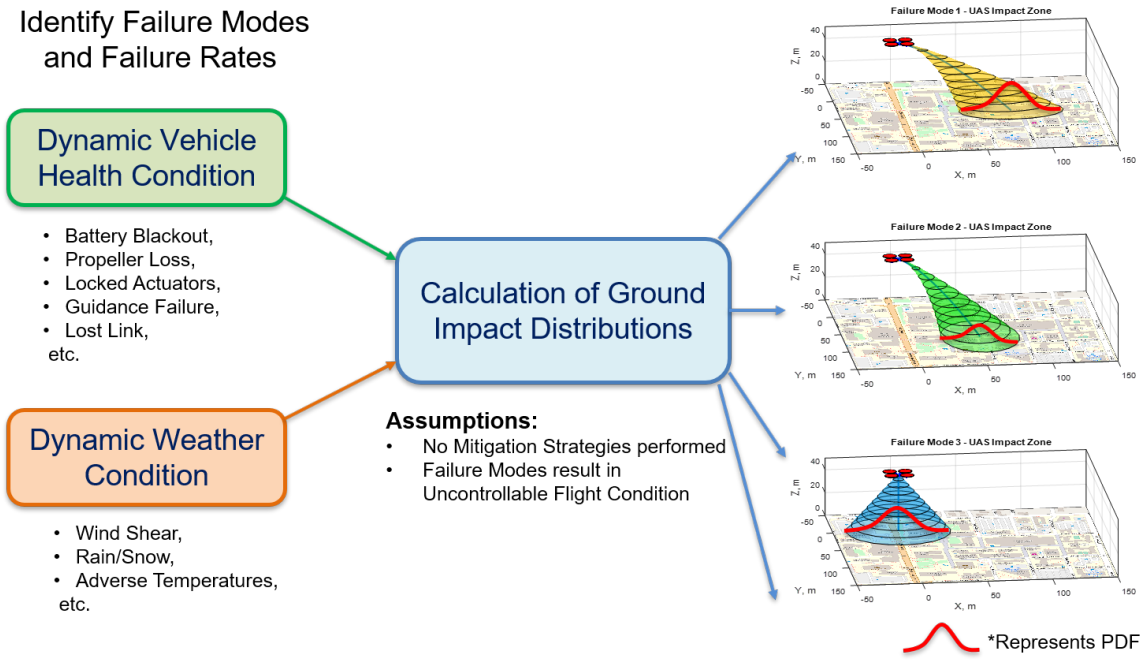

Figure 2.8: Calculation of ground impact distributions is depicted in flow chart

In this Figure, the UAS failure modes are grouped under two main categories which are the failure modes resulted from the dynamic vehicle health conditions and the dynamic weather conditions. Using failure mode analyses for these categories, it is proposed that the ground impact location distribution can be calculated under some assumptions.

Failure occurring on an aircraft system can result in two operational conditions, namely controllable flight and uncontrollable flight. While the normal mission can still be maintained or mitigation strategies can be performed in a controllable flight, in an uncontrollable flight, the mission is terminated by the loss of control on the system with a potential crash scenario. In this thesis, all the failure modes are presumed to result in an uncontrollable flight, and no mitigation strategies are performed. The resulting behavior of the UAS after a failure is analyzed regarding the impact location distribution over an area on the ground. Impact location is defined to be that in an uncontrollable flight condition, a position on the ground that UAS can reach from its current state where the failure occurs.

Impact domain of UAS is represented by a probability distribution over the ground locations for a given uncontrollable flight condition UF occurred at the current state of the vehicle $X(t)$, and at the current environmental conditions $E(t)$, $p(x|UF(X, E, t)$. Domain depends on the capabilities of the vehicle such as operating speed and available power on-board, and environmental conditions like wind direction and magnitude, which are investigated under the vehicle health condition category. In case of diminished capability modes such as a sensor, actuator or system unit failures, the range or endurance will be adversely affected too. Also, it is worth to note here that the presence of strong weather conditions can significantly alter the range and endurance of the UAS platform. Therefore, environmental conditions should be considered to determine the size and shape of the impact domain. This approach can

be used to determine probability density of impact locations over the map under each possible failure case according to their occurrence probabilities, and the mixture of these distributions will provide the probability distribution of impact locations for all failure modes over the map. As it is explained in Section 2.3.1, impact probability distribution of all failure modes is formulated as a mixture distribution. Equation (2.5) shows the formulation of mixture distribution.

$$p(x|UF(X,E,t)) = \sum_{j=1}^{k} \Big[p(x|F_j, UF(X,E,t))\Big] \Big[P(F_j|UF(X,E,t))\Big] \tag{2.5}$$

where $p(x|F_j, UF(X,E,t))$ is the probability density function that represents a UAS ground impact probability distribution over the map given that uncontrollable flight UF is caused by the jth failure mode F_j, at the current state of UAS, $X(t)$, and environmental conditions $E(t)$. $P(F_j|UF(X,E,t))$ is the conditional probability of the jth failure mode to cause uncontrollable flight at given conditions among all failure modes. Also, k is the total number of UAS failure modes.

As it is explained before, the occurrence of failure modes can depend on many factors. Hence, the current vehicle states, environmental conditions and time are included in conditional probabilities to address some of those factors. Using mixture distribution, the probability of UAS impact to a particular area A given a failure happened at a specific state and condition can be obtained by below integral.

$$P(A|UF(X,E,t)) = \int_A p(x|UF(X,E,t))\, dx \tag{2.6}$$

In addition, considering the density of uncontrollable flight condition to occur at a given specific vehicle state and environmental conditions $\lambda_{UF}(X,E,t)$, $UF(X,E,t)$ term can be eliminated from the condition in Equation (2.6).Then, UAS ground impact density to an area A can be obtained given the current time as

$$\lambda_{Impact}(A,t) = \lambda_{UF}(X,E,t)\ P(A|UF(X,E,t)) \tag{2.7}$$

Note that, the reason why the density of uncontrollable flight condition is used instead of probability is that for any exact $X(t)$ and $E(t)$, the probability of observing UF is zero since it is a continuous random process. $\lambda_{UF}(X,E,t)$ models the effect of time-varying vehicle states and environmental conditions on uncontrollable flight condition occurrences.

A simple sketch to illustrate the ground impact distribution of UAS platform is shown in Figure 2.9. In this sketch, four arbitrary failure modes are considered, and the impact distributions of the failure modes are modeled with truncated Gaussian distributions where the boundaries of the impact domains are assumed to be within the 3σ deviation of elliptical regions depicted in Figure 2.9(a). According to these failure ground impact distributions, the result of the calculation given in Equation (2.6) is plotted in Figure 2.9(b) where the occurrence rates of individual failure modes are selected as 10^{-5}, 10^{-4}, 10^{-3}, and 10^{-4} per hour, respectively.

2.3.3 Risk Function

In this section, quantification of the ground risk due to UAS operations will be derived as a risk function using the risk of exposure of the ground (PREM) and the UAS ground impact distributions which are explained from the previous sections. Derived risk function is the crucial component of the proposed risk assessment framework, and it will later be used as a cost function of the path planning algorithm while assessing the ground risks over planned trajectories.

There are a few scenarios that a risk condition can arise due to UAS operations. The obvious one is the crash scenarios of the platform or uncontrolled deviation of its planned trajectory such that the platform can pose a threat to the ground. These

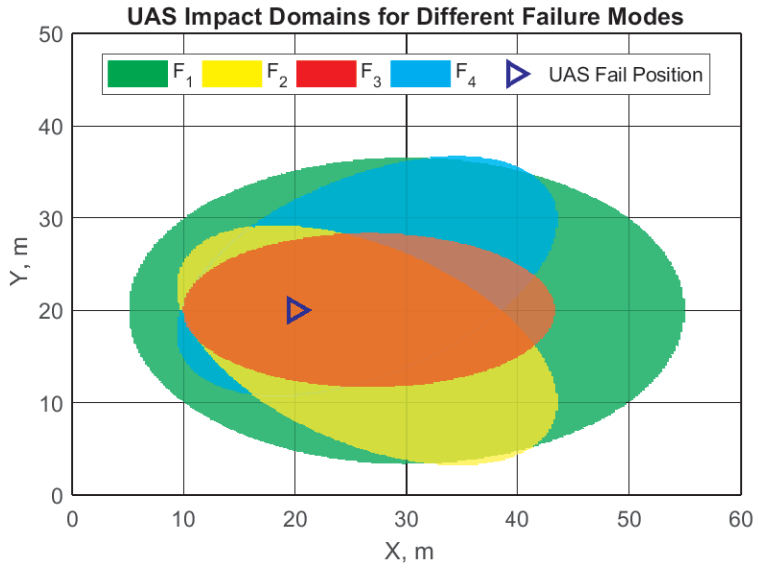

(a) Impact domains of failure modes - separately

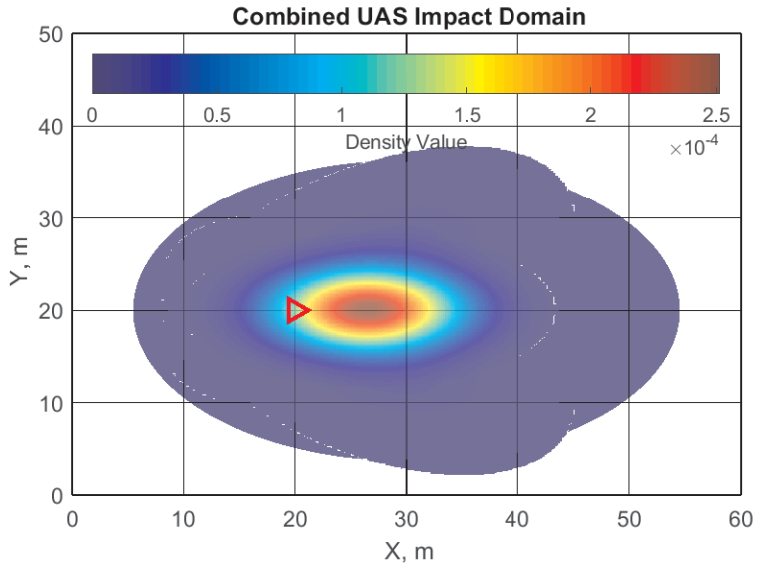

(b) Combined ground impact probability distribution

Figure 2.9: Failure mode impact domains and combined ground impact probability distribution

scenarios are categorized as the event-based risk conditions in this thesis. However, there are other scenarios causing risk conditions that are not event-based such as privacy intrusions. This category has not been fully defined yet, and it is still an open

debate. Therefore, the proposed risk assessment framework is modeled for only the event-based risk conditions, more specifically for the events causing platform impacts to the ground. Nonetheless, the flexibility of the previously introduced concepts and below framework can easily allow us to cover the other scenarios as mentioned earlier. This work utilizes the risk exposure map of the area (PREM) considering UAS failure modes and their ground impact probability distributions to quantify the risk of UAS platform impact risk to the ground. First, time parameterized density of the risk condition over the ground locations is derived in Equation (2.12) along the UAS trajectory. Then, the total risk of UAS impact along the path is formulated as the integration of risk densities and event probabilities with respect to time in Equation (2.14). Finally, the risk function (or cost) is formulated in Equation (2.14) for the path planner.

Equation (2.8) describes the calculation of uncontrollable UAS flight condition risk to a location x given that this flight condition is occurred at the current state of the vehicle, X and environmental conditions, E at time t. Basically, given the information where and when the UAS failed, impact risk on the ground is estimated by using the spatial distribution of impact probabilities and the expected value of the total risk condition at the impact location as

$$\begin{aligned} Risk(x \mid UF(X,E,t)) = & \\ & = Pr(\text{Impact to } x \mid UF(X,E,t)) \times \mathbb{E}[\text{Risk of impact to } x] \\ & = P(x \mid UF(X,E,t)) \Big[\int_{A_{platform}} PREM(u \mid x)\, du \Big] \end{aligned} \tag{2.8}$$

where $A_{platform}$ is the area on the ground that is affected by the platform impact to the location x. Impacted area, depending on the collision type, could be the size of

the platform, a smaller or larger area. Using the above relation, risk of UAS impact to impact domain defined for the given failure condition can be calculated.

Assuming that a UAS failure mode is modeled by a uniform impact distribution with a circular impact domain on the ground, the integration of a sample PREM and ground impact distribution to calculate point impact risks is shown in Figure 2.10 where the plot on the left depicts the $PREM$ and the UAS impact distribution on the ground. In the right plot, the spatial distribution of the impact risk is sketched.

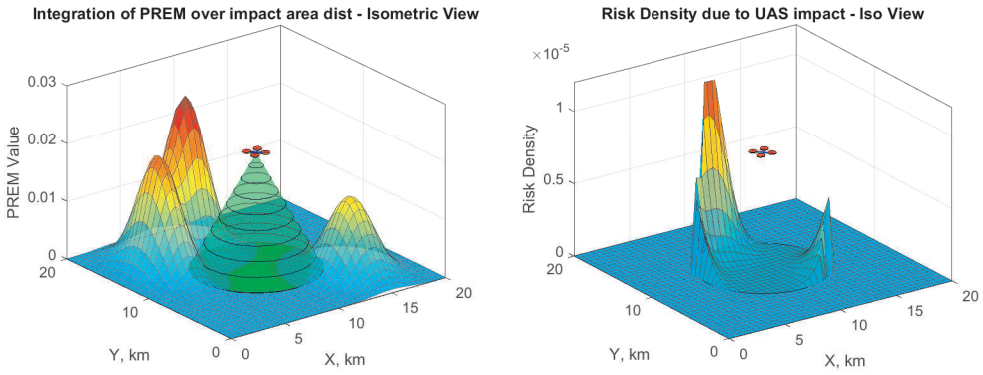

Figure 2.10: Illustration of a failure event with $PREM$ and impact distribution (left) and the calculation of the risk of a point on the discritized failure area (right)

As it can be seen, risks on the grids where impact domain intersects with high-risk regions have higher expected impact risk. Also, note that, at the outside of the impact domains, there is no risk expected since those regions are not reachable by the failing vehicle. Furthermore, total corresponding risk for this failure condition can be obtained by the area integral covering whole impact domain as below

$$\begin{aligned} Risk(A_{F_j} \mid F_j, UF(X,E,t)) = \\ = \int_{A_{F_j}} P(x \mid F_j, UF(X,E,t)) \left[\int_{A_{platform}} PREM(u \mid x)\, du \right] dx \end{aligned} \tag{2.9}$$

where A_{F_j} is the impact domain area of the jth failure mode F_j.

Including all the failure modes, above equation can be updated using the conditional probability of individual failure modes in Equation (2.10).

$$\begin{aligned} &Risk(A_F \mid UF(X,E,t)) = \\ &\qquad = \sum_{F_j \in F_{all}} P(F_j \mid UF(X,E,t))\ Risk(A_{F_j} \mid F_j, UF(X,E,t)) \end{aligned} \tag{2.10}$$

where A_F is the total impact domain area of all the failure modes.

Equation (2.10) requires the uncontrollable flight condition to be known in advance to compute the total risk for an impact scenario. On the other hand, the occurrence rate of the UF condition can be included in the risk calculation as it is introduced in Equation (2.7). By so, impact risk density to the ground caused by the presence of a UAS at a specific state and environmental condition can be expressed as follows

$$RiskDensity(X,E,t) = \lambda_{UF}(X,E,t)\ Risk(A_F \mid UF(X,E,t)) \tag{2.11}$$

The open form of the Equation (2.11), which calculates the total risk due to UAS failures occurring at the current conditions and time, shown in Equation (2.12).

$$\begin{aligned} &RiskDensity(X,E,t) = \\ &\quad = \lambda_{UF}(X,E,t) \sum_{F_j \in F_{all}} P(F_j \mid UF(X,E,t)) \\ &\qquad \left[\int_{A_{F_j}} P(x \mid F_j, UF(X,E,t)) \left[\int_{A_{platform}} PREM(u \mid x)\, du \right] dx \right] \end{aligned} \tag{2.12}$$

Impact risk density due to the current state of the UAS platform and the environmental conditions is found by multiplying the occurrence rate of uncontrollable

flight at $X(t)$ and $E(t)$ by the summation of the risk conditions due to individual failure modes. Individual risk conditions are found by the integral of the conditional impact probability distribution of UAS given a failure condition occurring at given conditions multiplied by the nested integral of PREM defined over the platform impact area given the crash location x. Then, this calculation is repeated for each failure modes. The result of Equation (2.12) is a unit-less rate. However, if the PREM layer has a quantitative measure for corresponding risk condition, such as the number of people affected, then it can be used as a unit of the impact risk density. An example can be given as the number of people hit by a UAS platform per flight hour.

Using the formula derived in Equation (2.12), the risk level of the UAS path can be computed by integrating the impact risk densities along the trajectory. It is important to point out that this integration implies that failures are assumed to be occurring in every time step. Clearly, this assumption is not correct because, after the first failure case, vehicle cannot proceed the normal operation, and so, the risk that corresponds to the remaining part of the path, after the occurrence of failure, cannot be included in total risk. For the correct integration of total risk, the probability of not having any failure in a given time period should be known until reaching the goal. The risk level of the UAS path is given in Equation (2.13).

$$Risk = \int_0^{T_{Path}} P(\neg UF(X, E, t)) RiskDensity(X, E, t)\, dt \tag{2.13}$$

where T_{Path} is the total elapsed time until UAS reaches its destination. $P(\neg UF(X, E, t))$ is the probability that no failure occurred until time t.

The probability term, $P(\neg UF(X, E, t))$, can also be seen as the discounting factor in future risks. It means that the risk in the near future has a higher weight (or importance) than the risk in the distant future during the risk calculation.

If failure modes are assumed to be following the Poisson distribution with constant failure rates, Equation (2.13) can be reconstructed as

$$Risk = \int_0^{T_{Path}} e^{-\lambda t} RiskDensity(X, E, t)\, dt \tag{2.14}$$

where $\lambda = \sum_j \lambda_j$ is the summation of individual failure mode rates following Poisson distribution. Note that, Poisson distribution with zero event has exponential decay ($P(X(t) = 0) = e^{-\lambda t}((\lambda t)^0)/0!$).

This assumption implies that the occurrence of failures is constant regardless of the vehicle state and environmental conditions, which is the oversimplification of the actual process. Nevertheless, for the practical simulation purposes, this assumption will be employed in this thesis.

As it can be noticed, Equation (2.13) is basically in the form of performance index, which is widely known and used in optimal control theory, as below.

$$J = \phi(x(t_0), t_0) + \psi(x(t_f), t_f) + \int_0^{t_f} L(t, x, u)\, dt$$

where t_0 and t_f are the initial and final time of the solution, and the first two terms represent the cost of the initial and final states of the solution. $L(t, x, u)$ function is used to account for the cost of following a specific trajectory such as total distance traveled or the duration. It is selected to be the total risk of following a path with the term inside the integral in Equation (2.13) to construct the risk function for the proposed risk assessment.

CHAPTER 3

PATH PLANNING ALGORITHMS

In this chapter, rapidly-exploring random tree (RRT) path planning algorithms will be reviewed and explained shortly including the simple heuristics approaches and a path optimization method that are used during the simulations in Chapter 5.

The path planning is one of the most studied topics by many different fields from robotics to biochemistry and plenty of other areas by various communities. It still attracts a considerable amount of attention from researchers seeking answers to challenging and fundamental questions in path planning. The purpose of the path planning, in general, can be defined as finding a collision-free route that connects the initial configuration of the agent to the desired goal configuration, which is a purely geometric process regardless of dynamic feasibility of the found path. In the literature, there are numerous categorizations of the path planning algorithms such as global versus local planners, deterministic versus probabilistic planners, or conventional versus advanced hybrid methods. Victerpaul et al. investigated and compared the traditional path planning methods such as artificial potential field, graph search, and road map techniques, and the other advanced planning methods such as genetic algorithm, neural network and fuzzy logic techniques in their comprehensive survey study in [21]. On the other hand, Elbanhawi in his review work, [22], scrutinized the sampling-based probabilistic methods such as probabilistic road maps (PRMs) and rapidly-exploring random trees (RRTs) used in the robotics field. He concludes that as the state-of-art methods, sampling-based path planning techniques are more promising and capable of overcoming some of the challenges that conventional or the other

algorithms suffer from. Especially for the systems with high dimensional workspace or the clutter environment, it is shown that the randomized sampling-based algorithms outperform the deterministic approaches such as cell decomposition, Voronoi diagrams and graph search algorithms (A* and Dijkstra) in his work. Various other works from distinct communities support these findings and improved variations of these algorithms are introduced later on, [23, 24, 25].

Due to its generality, easiness, and high performance in many applications, RRT algorithms are adopted in this thesis work to incorporate with the proposed risk assessment framework. Although the basics of the RRT algorithms and used heuristics will be covered in this chapter, the reader is strongly suggested to review the reference studies and previous work to acquire deep knowledge about the path planning algorithms.

3.1 RRT Algorithms

The rapidly-exploring random tree is a sampling-based efficient search algorithm that incrementally grows a tree from the initial configuration to the goal configuration. It is basically a space-filling tree, which covers the configuration space by sampling random configurations and extending tree branches iteratively. Due to the nature of the tree structure, RRT is a single-query planner, which means once the solution is found, there is only one path between initial and goal configuration. The simple RRT algorithm with a uniformly random sampling strategy is inherently biased towards unexplored regions (largest Voronoi regions), and it rapidly explores these regions as its name states.

These algorithms are proven to be probabilistically complete, [26], which is a weaker notion of completeness in path planning. It means that if a solution exists, the probability of the algorithm to find it will approach to the one as the runtime

approaches to the infinity. Some of the advantages of these algorithms can be listed as the easy implementation in most of the general systems, efficient search in high dimensional spaces, and easy representation of the obstacles and dynamical constraints. These properties make sampling-based methods popular among many researchers for their rapid implementations. Although having favorable properties, these algorithms have also several drawbacks. The solution of the planning problem is highly sensitive to the metric used in the path evaluation and tree construction. Another disadvantage is the difficulty of predicting the convergence rate of the algorithm due to random factors. Therefore, the time required to compute a path is generally unknown and can be affected by the selection of the parameters. Despite such drawbacks, significant success has been achieved in the practical applications of sampling-based algorithms, especially with RRTs.

In below sections, starting from the simplest version, four different variations of RRT algorithms, which are RRT, RRT*, bi-RRT* and multi-RRT*, will be summarized with their pseudo-codes and sketches.

3.1.1 RRT

The simplest version of the rapidly-exploring random tree algorithms, RRT, is first introduced by LaValle in [27]. The pseudo-code of the algorithm is given in Algorithm 1 and Figure 3.1 illustrates how the algorithm proceeds.

RRT starts with initializing the tree at the initial configuration node, which is often called the root node. Then, inside the main loop, the algorithm proceeds as follows. Firstly, a random configuration is sampled from the configuration space, depicted in Figures 3.1(a) and 3.1(c). Secondly, the nearest node on the tree to the sampled node is found and using the EXTEND function a new tree branch (new configuration) is extended considering the maximum extension step size, Figures 3.1(b)

Algorithm 1 RRT

Input: $q_{init}, q_{goal}, maxIter, stepSize, \mathcal{C}_{free}$, Obst, $Threshold$

Output: Path, Tree

Tree.init(q_{init})

1: **for** $i = 1$ to $maxIter$ **do**

2: $q_{rand} \leftarrow$ RAND_NODE($\mathcal{C}_{free}$)

3: $q_{nearest} \leftarrow$ NEAREST_NODE(q_{rand}, Tree)

4: $q_{new} \leftarrow$ EXTEND($q_{nearest}, q_{rand}, stepSize$)

5: $q_{new}.Parent \leftarrow q_{nearest}$

6: $cost_{new} \leftarrow cost_{nearest} + c(q_{nearest}, q_{new})$

7: **if** COLLISION_CHECK(q_{new}, Obst) **then**

8: Tree.ADD_NODE($q_{new}, cost_{new}, [q_{new}.Parent, q_{new}]$)

9: **if** $Dist(q_{new}, q_{goal}) < Threshold$ **then**

10: Path $\leftarrow$ BACKTRACK(q_{new}, Tree)

11: MultiPath(end+1) = Path (*or* **break**)

12: **end if**

13: **end if**

14: **end for**

15: **return** Path, Tree

and 3.1(d). In Line 5 and 6, the nearest node on the tree is appended as the parent node of the new configuration, and the cost of this extension step is found. After that, this newly extended node is checked whether it collides with obstacles, and if it is not colliding, this node is officially added to the tree as the new node with its parent and extension cost properties. This procedure repeats until either a new extension gets inside the threshold radius of the goal configuration, Line 9 and Figure 3.1(e), or the

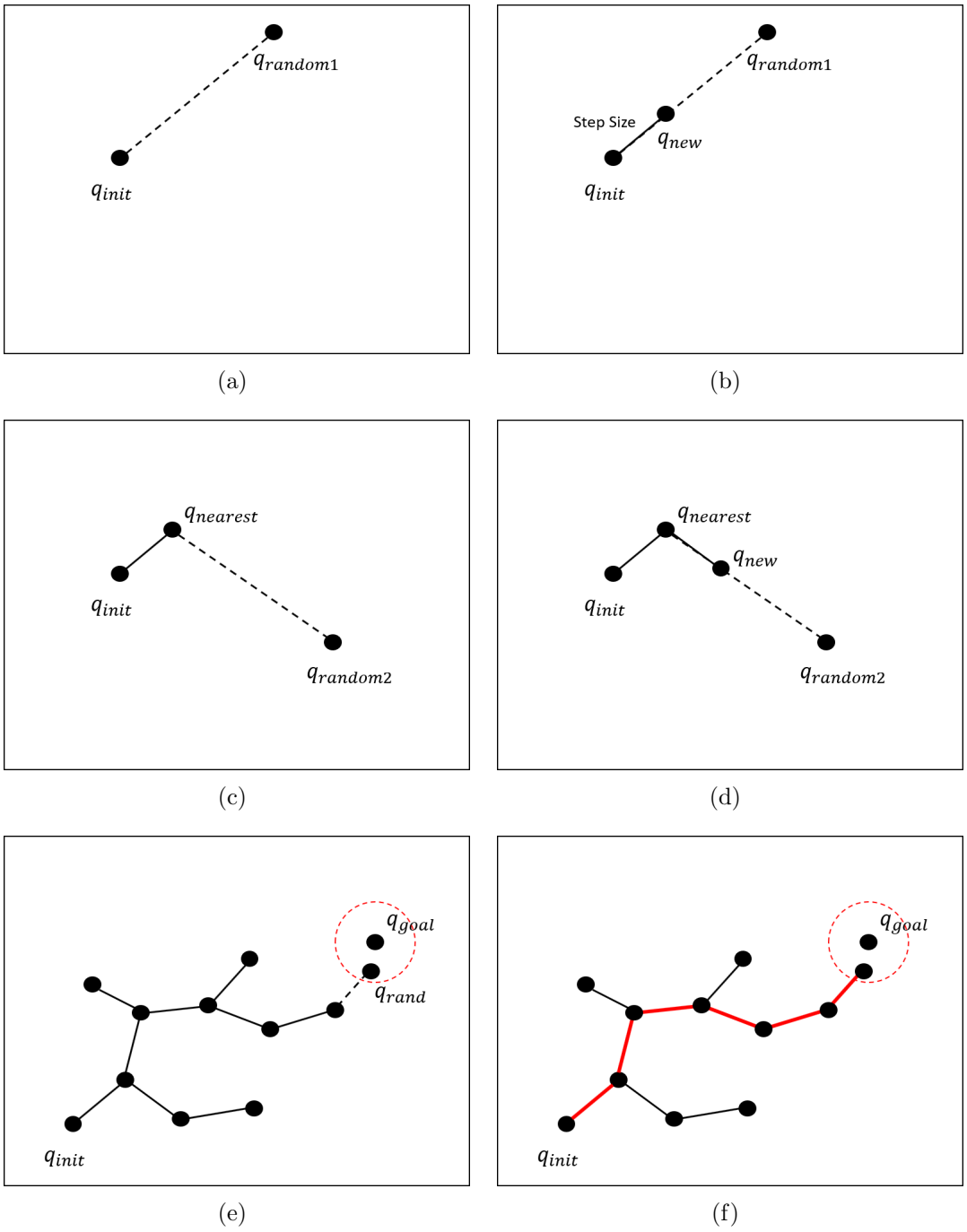

Figure 3.1: Illustration of simple RRT algorithm

maximum iterations are reached. If any of the extension reaches the proximity of the destination, the backtracking function creates the path by tracking the nodes back

using the parent information until reaching the root node, Line 10 and Figure 3.1(f). It is important to note in Line 11 that the RRT algorithm can either be stopped when the first path is found or be continued by saving the found multiple paths until reaching maximum iteration limit. The difference between these two approach will be discussed in the path optimization section.

This basic algorithm forms the backbone of the subsequent RRT algorithms. Therefore, the below subsections regarding the other variations of RRT will only explain the additions or modifications made on top of this algorithm.

3.1.2 RRT*

A significant extension to the simple RRT algorithm is introduced with RRT* by Karaman in [23, 28], which adds the asymptotic optimality property to the algorithm by employing a "Rewiring" operation. The pseudo-code of the RRT* can be seen in Algorithm 2, where the only difference from the standard RRT is just the addition of near node calculation and the REWIRE function in Line 8 and 9.

Rewiring operation is defined to be the rewiring of the existing tree branches (modifying parent relations of the nodes) to achieve the lowest accumulative cost along the path, and it is applied in every iteration to the specific tree nodes which are the near nodes of the last extended node. REWIRE function is explained in Algorithm 3, and the procedure is depicted in Figure 3.2.

Rewiring function takes the newly extended node, q_{new}, and the near nodes, Q_{near}, that are found within the ball of radius, k, of the extended node with their corresponding extension costs. The ball of radius is calculated according to the Equation (3.1). (Details can be found in [28, 22])

$$k = \gamma \Big(\frac{log(n)}{n} \Big)^{\frac{1}{d}} \tag{3.1}$$

Algorithm 2 RRT*

Input: $q_{init}, q_{goal}, maxIter, stepSize, \mathcal{C}_{free}$, Obst, $Threshold, R$

Output: Path, Tree

Tree.init(q_{init})

for $i = 1$ to $maxIter$ **do**
  $q_{rand} \leftarrow$ RAND_NODE($\mathcal{C}_{free}$)
  $q_{nearest} \leftarrow$ NEAREST_NODE(q_{rand}, Tree)
  $q_{new} \leftarrow$ EXTEND($q_{nearest}, q_{rand}, stepSize$)
  $q_{new}.Parent \leftarrow q_{nearest}$
  $cost_{new} \leftarrow cost_{nearest} + c(q_{nearest}, q_{new})$
  if COLLISION_CHECK(q_{new}, Obst) **then**
    $[Q_{near}, COST_{near}] \leftarrow$ NEAR_NODES(q_{new}, Tree, R)
    Tree $\leftarrow$ REWIRE($q_{new}, cost_{new}, Q_{near}, COST_{near}$, Tree)
    if $Dist(q_{new}, q_{goal}) < Threshold$ **then**
      Path $\leftarrow$ BACKTRACK(q_{new}, Tree)
      MultiPath(end+1) = Path (*or* **break**)
    end if
  end if
end for
return Path, Tree

Where γ is a distance parameter, n is the number of current nodes in the tree, and the d is the number of dimensions of the configuration space. This formula implies that as the tree grows, the radius of near node search is logarithmically decreasing. In addition, the selection of the γ is affected by the path planning environment and the cost metric.

Algorithm 3 REWIRE

Input: $q_{new}, cost_{new}, Q_{near}, COST_{near}$

Output: Tree

1: $c_{min} \leftarrow cost_{new}$
2: **for** $q_{near} \in Q_{near}$ **do**
3: $c_{new} \leftarrow cost_{near} + c(q_{near}, q_{new})$
4: **if** $c_{new} < c_{min}$ **then**
5: $q_{new}.Parent \leftarrow q_{near}$
6: $c_{min} \leftarrow c_{new}$
7: **end if**
8: **end for**
9: Tree.ADD_NODE$(q_{new}, c_{min}, [q_{new}.Parent, q_{new}])$
10: **for** $q_{near} \in Q_{near}$ **do**
11: $c_{min_{near}} \leftarrow cost_{near}$
12: $c_{near} \leftarrow cost_{new} + c(q_{new}, q_{near})$
13: **if** $c_{near} < c_{min_{near}}$ **then**
14: $q_{near}.Parent \leftarrow q_{new}$
15: $c_{min_{near}} \leftarrow c_{near}$
16: Tree.MODIFY_NODE$(q_{near}, c_{min_{near}}, [q_{near}.Parent, q_{near}])$
17: $UpdateChildrenNodeCosts(q_{near}, \text{Tree})$
18: **end if**
19: **end for**
20: **return** Tree

Rewiring consists of two steps. In the first step, Line 1-9, the best parent among the near nodes to connect the new node is searched according to their extension costs

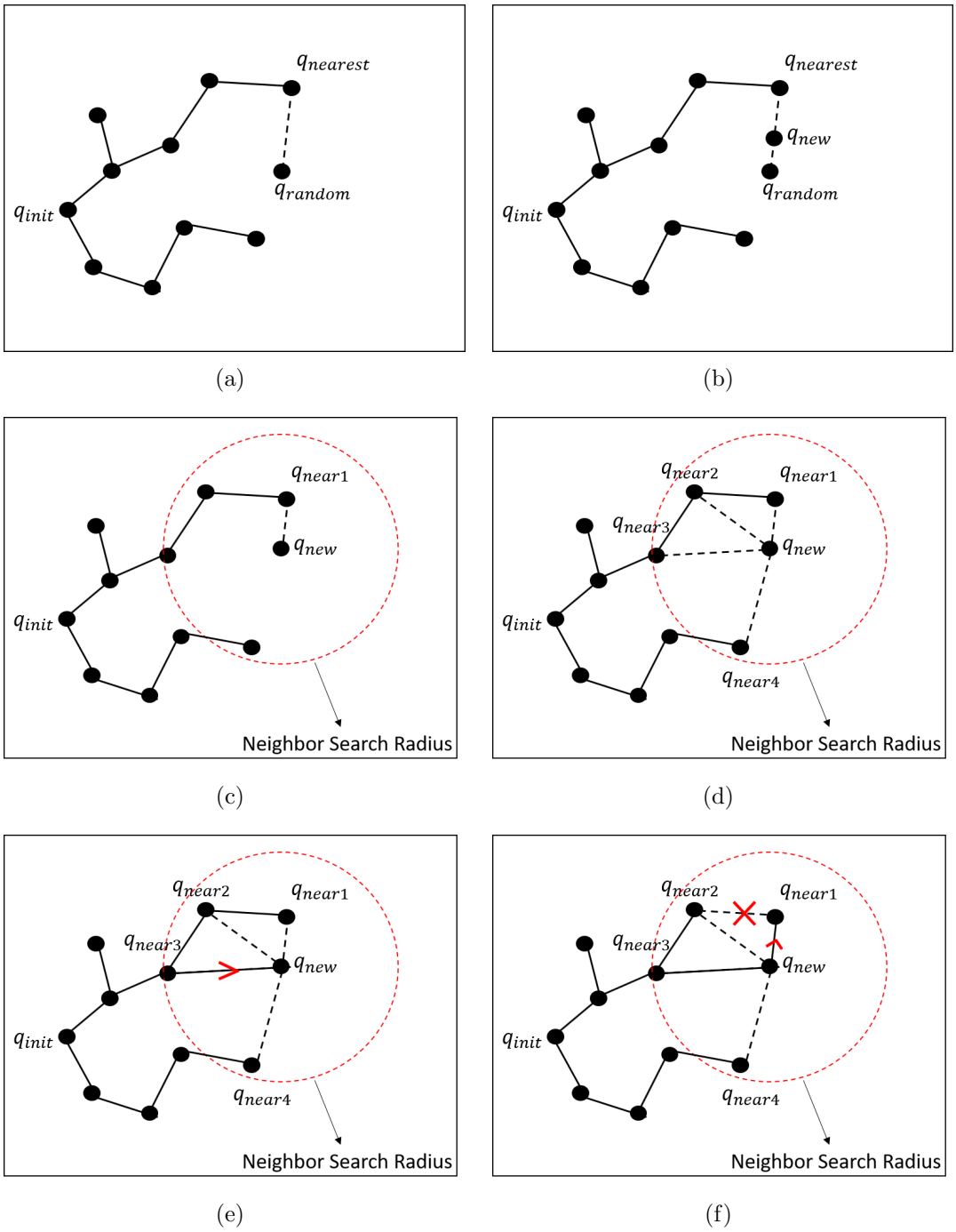

Figure 3.2: Illustration of rewiring operation of RRT* algorithm

compared to the current parent of the new node, which was the nearest node. If there is any node that connects to the q_{new} with the lower accumulated cost, the parent of

the new node is updated to corresponding near node as depicted in Figures 3.2(d)-3.2(e). In the second step, Line 10-20, the new node itself is considered whether it would be a better parent or not for each one of the near nodes separately. This basically means that if traveling along the new node to reach a near node has lower accumulated cost than the original accumulated cost of that near node, the previous parent of that near node is removed and the new node is assigned to be the parent for that near node as illustrated in Figure 3.2(f), where the parent of q_{near_1} is modified.

The rewiring operation applied in every iteration ensures the locally optimal connections between nodes and incremental optimization in global. As in the case of probabilistically completeness, these incremental optimizations satisfies the global optimality as the iterations approach to the infinity. However, it is also important to note that the selection of the near node calculation parameters has a direct effect on the path solution and the complexity.

3.1.3 Bi-RRT*

Another variation of the RRT* algorithm with two bidirectional trees, Bi-RRT*, is introduced by Jordan and Perez in their work [24]. The algorithm is the same as the RRT* except for having two different trees, forward and backward trees. The forward tree is initialized at the initial configuration, whereas the backward tree grows from the goal configuration. Each successful connection between these two trees forms a path that connects the initial configuration to the goal configuration. The main advantage of having two trees is the elimination of the need to reach the proximity of the goal configuration to connect. Instead, every node on both trees can be a candidate for the connection, which increases the efficiency of the search. The pseudo-code of Bi-RRT* is given in Algorithm 4, and Figure 3.3 illustrates the connection of bidirectional trees.

Algorithm 4 Bi-RRT*

Input: $q_{init}, q_{goal}, maxIter, stepSize, \mathcal{C}_{free}$, Obst, $Threshold, R$

Output: Path, ForwardTree, BackwardTree

ForwardTree.init(q_{init})

BackwardTree.init(q_{goal})

1: **for** $i = 1$ to $maxIter$ **do**

2: $q_{target} \leftarrow$ CHOOSE_TARGET($\mathcal{C}_{free}, BackwardTree$)

3: $q_{nearest} \leftarrow$ NEAREST_NODE(q_{target}, ForwardTree)

4: $q_{new} \leftarrow$ EXTEND_FORWARD($q_{nearest}, q_{target}, stepSize$)

5: $q_{new}.Parent \leftarrow q_{nearest}$

6: $cost_{new} \leftarrow cost_{nearest} + c(q_{nearest}, q_{new})$

7: **if** COLLISION_CHECK(q_{new}, Obst) **then**

8: $[Q_{near}, COST_{near}] \leftarrow$ NEAR_NODES(q_{new}, ForwardTree, R)

9: ForwardTree $\leftarrow$ REWIRE_FORWARD($q_{new}, cost_{new}, Q_{near}, COST_{near}$, ForwardTree)

10: **if** CONNECTION_CHECK((q_{new}, q_{goal}, ForwardTree, BackwardTree, $Threshold$) **then**

11: Path $\leftarrow$ BIDIRECTIONAL_BACKTRACK(q_{new}, ForwardTree, BackwardTree)

12: MultiPath(end+1) = Path (*or* **break**)

13: **end if**

14: **end if**

15: Repeat the lines 2-14 for the BackwardTree using _BACKWARD Functions

16: **end for**

17: **return** Path, ForwardTree, BackwardTree

In the algorithm, _FORWARD and _BACKWARD notations are used to identify the functions specific to the forward and backward trees in case that the computations

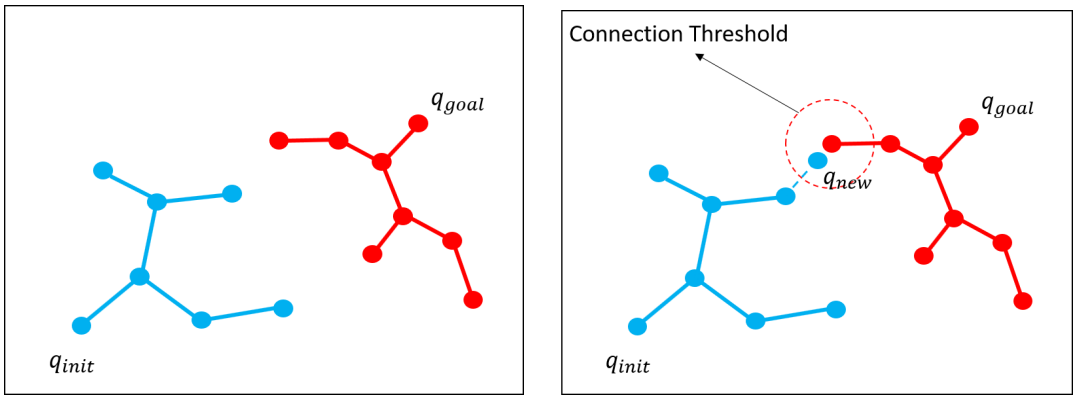

(a) (b)

Figure 3.3: Illustration of the connection between trees in Bi-RRT* algorithm

might differ for each one. The difference between the RRT* and Bi-RRT* algorithms, as previously stated, is the connection between both tree branches. To construct the path from the connection nodes, bidirectional backtracking function is used in Line 11. This function backtracks the forward and backward tree separately until reaching the initial node and the goal node respectively, and then, creates the path using the parent node relations along the trees and propagating the accumulated cost along the path.

In addition, CHOOSE_TARGET function, in Line 2, can be used to guide the extension of the trees toward each other by biasing the random sampling to generate sample nodes on the reverse tree. This procedure will be explained later in the heuristics subsection.

3.1.4 Multi-RRT*

Multi-RRT* is an extension to the Bi-RRT* which can employ more than two bidirectional trees to find the path solutions, as implemented in [25, 29]. The main difference is that Multi-RRT* can have multiple backward trees stem from different goal configurations, while the Bi-RRT* has only one backward tree. Each one of

the forward and backward tree pairs in Multi-RRT* algorithm can be considered as separate Bi-RRT*s which means the backward trees are allowed to connect only the forward tree, not to each other as illustrated in Figure 3.4. The advantages of having multiple pairs of bidirectional trees are the multiple goal selection, multi-objective planning and fast coverage of the configuration space. However, there are a couple of drawbacks as well such as the increased complexity in time and space, and inefficient space filling in overlapping backward tree regions. Nevertheless, its practical implementations show that these algorithms can efficiently solve multi-objective optimization problems in high-dimensional spaces and highly clustered environments. The pseudo-code of the Multi-RRT* is given in Algorithm 5.

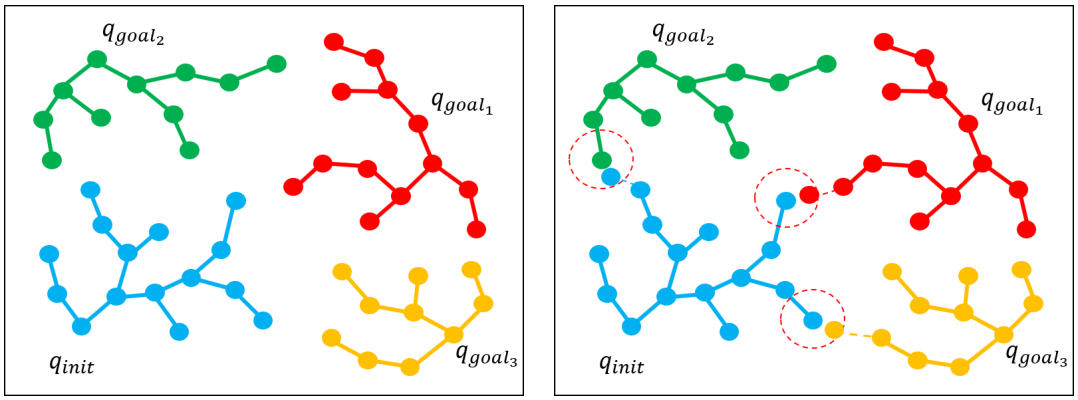

(a) (b)

Figure 3.4: Illustration of multi-tree RRT* algorithm

In this algorithm, bidirectional tree extensions occur similarly, except that in Line 15-17, multiple backward trees are extended in a loop during each iteration.

Algorithm 5 Multi-RRT*

Input: $q_{init}, Q_{goal}, maxIter, stepSize, \mathcal{C}_{free}$, Obst, $Threshold, R$

Output: Path, ForwardTree, BackwardTrees

ForwardTree.init(q_{init}), BackwardTrees.init(Q_{goal})

1: **for** $i = 1$ to $maxIter$ **do**
2: $q_{target} \leftarrow$ CHOOSE_TARGET($\mathcal{C}_{free}, BackwardTrees$)
3: $q_{nearest} \leftarrow$ NEAREST_NODE(q_{target}, ForwardTree)
4: $q_{new} \leftarrow$ EXTEND_FORWARD($q_{nearest}, q_{target}, stepSize$)
5: $q_{new}.Parent \leftarrow q_{nearest}$
6: $cost_{new} \leftarrow cost_{nearest} + c(q_{nearest}, q_{new})$
7: **if** COLLISION_CHECK(q_{new}, Obst) **then**
8: $[Q_{near}, COST_{near}] \leftarrow$ NEAR_NODES(q_{new}, ForwardTree, R)
9: ForwardTree $\leftarrow$ REWIRE_FORWARD($q_{new}, cost_{new}, Q_{near}, COST_{near}$, ForwardTree)
10: **if** CONNECTION_CHECK((q_{new}, Q_{goal}, ForwardTree, BackwardTrees, $Threshold$) **then**
11: Path $\leftarrow$ BIDIRECTIONAL_BACKTRACK(q_{new}, ForwardTree, BackwardTrees)
12: MultiPath(end+1) = Path (*or* **break**)
13: **end if**
14: **end if**
15: **for** $k = 1$ to # of BackwardTrees **do**
16: Repeat the lines 2-14 for each BackwardTree using _BACKWARD Functions
17: **end for**
18: **end for**
19: **return** Path, ForwardTree, BackwardTree

3.2 Heuristics

In this section, three simple heuristics, which are goal biasing, transition test, and cost guided sample generation, that are used to increase the efficiency of the RRT algorithms are explained.

Heuristics are defined to be the basic notions that help finding solutions by making some assumptions about the solution environment and search process itself. However, these assumptions may not hold for any arbitrary planning process or systems, which is common in practice. Therefore, a heuristic may perform poorly if the underlying process does not satisfy the assumptions made. A standard approach to overcome this problem is to use the combination of different heuristics that perform well under varying conditions. In this thesis, sampling bias and rejection sampling heuristics will be combined and used in the path planning scenarios.

3.2.1 Goal Bias

Goal bias heuristic is one of the simplest sampling methods used in RRT algorithms. The basic idea is to deliberately guide the generation of samples near or at the goal configuration itself. This is usually achieved by employing a probability threshold to switch between random sampling and the goal biased samples. The sampling strategy is given in Algorithm 6.

The advantage of the goal biased samples is the generation of more samples near the goal configuration, which can yield a path solution potentially with a higher chance. However, this also means that this approach limits the exploration of the whole configuration space, and so, the other potential solutions might have been missed. This problem is defined as the exploration-exploitation trade-off. The selection of the goal bias, denoted by P_{goal}, determines how greedy the search will be. In usual practices, goal bias probability is selected around 0.1.

Algorithm 6 GOAL_BIAS

Input: $q_{goal}, \mathcal{C}_{free}, P_{goal}$

Output: q_{rand}

1: $p \leftarrow randomNumber([01])$

2: **if** $p < P_{goal}$ **then**

3: **return** $q_{rand} \leftarrow q_{goal}$

4: **else**

5: **return** $q_{rand} \leftarrow$ RAND_NODE($\mathcal{C}_{free}$)

6: **end if**

3.2.2 Transition Test

Transition test is a sampling rejection heuristic that is used to discard some of the generated samples according to a measure. The idea behind the test is that if a generated sample requires a transition from a low-cost node to a high-cost node (uphill), a rejection test is applied, and depending on how steep the cost transition is, test is either passed or failed which will determine whether to discard the sample or not. If the transition occurs from a high-cost node to a low-cost (downhill), the test is always passed. It is important to note here that the rejection measure on the test is an adaptive parameter. The adaptation law is designed such that after every extension trial along the uphill direction, if the test is passed, the rejection threshold is incrementally decreased to guide the search toward lower-cost regions, and if the test is failed, the rejection threshold is increased to relax the limits allowing the exploration on the high-cost regions. In basic words, the transition test guides the search toward lower cost regions first as much as possible by adaptively changing its rejection condition. The implementation details can be seen in these reference studies [25, 29]. The pseudo-code of the transition test is given in Algorithm 7.

Algorithm 7 TransitionTest

Input: Tree, $T, T_{rate}, cost_{new}, cost_{parent}$

Output: TestResult

1: **if** $cost_{new} \geq cost_{parent}$ **then**
2: **if** $exp(-(cost_{new} - cost_{parent})/T) > 0.5$ **then**
3: $T \leftarrow T/2^{(cost_{new} - cost_{parent})/\text{costRange(Tree)}}$
4: **return** TestResult $= True$
5: **else**
6: $T \leftarrow T \cdot 2^{T_{rate}}$
7: **return** TestResult $= False$
8: **end if**
9: **else**
10: **return** TestResult $= True$
11: **end if**

In this algorithm, T is called the Temperature that is used to calculate the rejection threshold in Line 2, and it is an adaptive parameter where the adaptation laws are given in Line 3 and 6. T_{rate} is a constant parameter that determines how fast the Temperature should be restored (increased).

3.2.3 PREM Guided Sample Generation

As a last heuristic that will be used in this work, PREM guided sample generation is explained. In this method, the random sample configurations are drawn from a specific distribution, where the risk exposure distribution (PREM) is selected in this case. Remember that the higher density in the PREM distribution corresponds to the higher exposures and potentially the higher cost nodes. To minimize the gen-

eration of the high-cost nodes, which will ensure the less costly paths, the samples with the low risk exposures should be generated. Therefore, the inverse relation of PREM distribution will be used to generate sample nodes.

The purpose of this sampling method is to reduce the tree growth to high-cost regions by simply not selecting any samples on them. However, one can notice that even though the samples are not drawn from the high cost regions, during the early extension process of the branches, nodes can be extended into the high-cost regions. This is simply due to the fact that if the randomly sampled configuration is far away from the nearest tree node, the simple RRT extension process can generate intermediate configuration where may coincide with a high-cost region between the nearest node and the sampled node. On the other hand, as the tree grows larger and covers most of the space, the intended strategy becomes more accurate since the distance between the nearest and sampled node are shorter. Therefore, PREM guided sample generation heuristic will be used along with the other heuristics. The generation of PREM guided samples is illustrated in Figure 3.5(a). The first figure is the contour plot of the underlying PREM, and the second figure demonstrates the sample nodes drawn from the inverse PREM distribution.

3.3 Path Optimization

Randomized path planners in general usually tend to yield non-smooth paths with zigzags and jerky path segments due to random sampling and extension processes since the dynamic (and sometimes kinematic) constraints of the vehicle are not considered by the majority of these path planning algorithms, except for the kino-dynamic planners. For this reason, after the path solution is found, it is common to use a path optimization technique to smooth out the path further. It is important to note here that various measures can quantify the smoothness of the path. Some

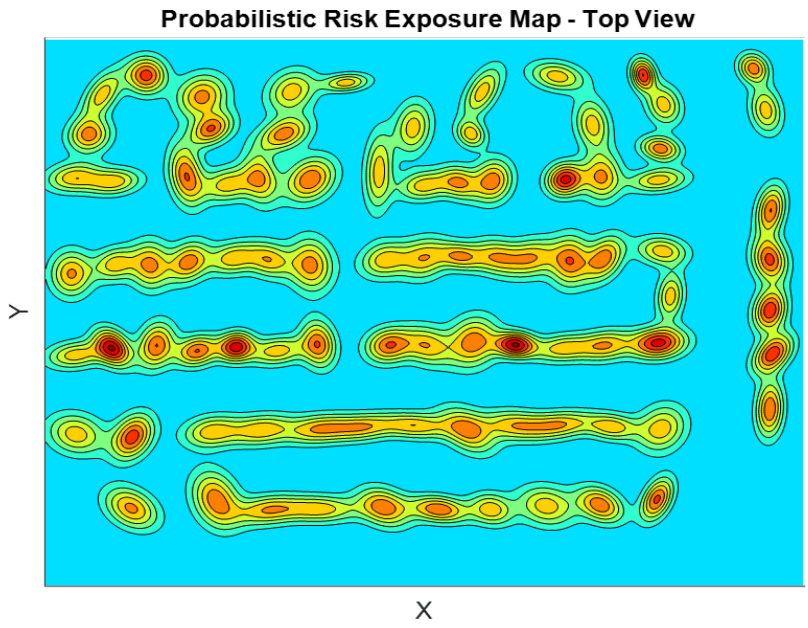

(a) PREM contour map

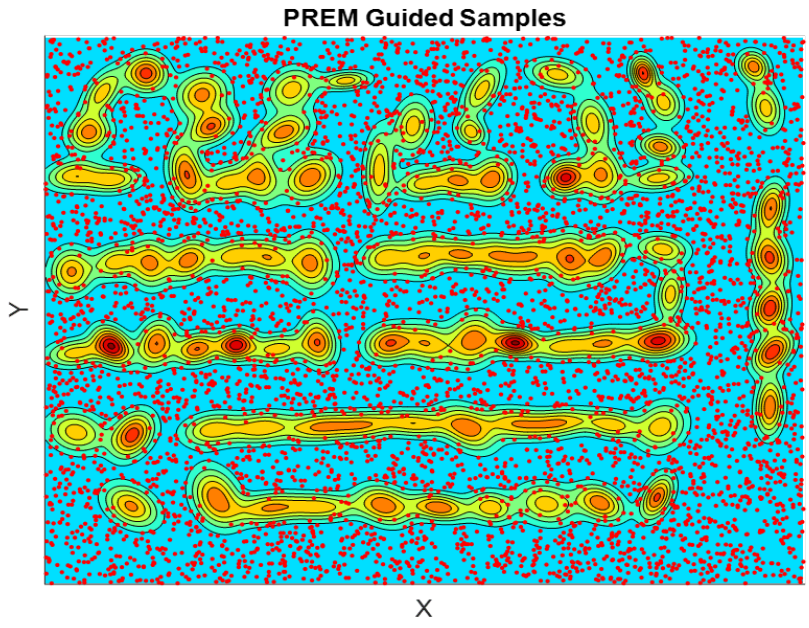

(b) PREM guided samples

Figure 3.5: Illustration of PREM guided sample node generation

of these measures are the Euclidean distance, time, or the other cost metrics. The combination of these measures can be incorporated as well. In this thesis, the consideration on the path solution is the total risk accumulated along the path. Thus, path optimization is expected to smooth the current path segments to yield even less risky paths if possible.

Remembering the RRT* algorithm, the rewiring operation itself is introduced as an optimization method, which locally optimizes the tree branches to yield less costly path segments, and by so an optimized path is obtained as the tree covers the configuration space. This brings us to ask the question of whether the rewiring technique can also be used more directly to optimize the path solution before generating enough samples to cover the whole configuration space.

In this thesis, the rewiring technique (* operation) is proposed to be used as a path optimization method. This is achieved by utilizing the exploration and exploitation steps according to the predefined conditions. Algorithm 8 describes the high-level iteration steps during the planning process.

Algorithm 8 Exploration-Exploitation Relation During Path Planning

```
1: StartExploitation = False, PathFound = False
2: for i to iterMax do
3:    [MultiPath, PathFound, StartExploitation] ← RRT* Exploration Step
4:    if PathFound ∧ StartExploitation then
5:       Path ← SELECT_PATH(MultiPath)
6:       OptimizedPath ← PATH_OPTIMIZATION(Path)
7:    end if
8: end for
9: return OptimizedPath
```

In this algorithm, RRT* Exploration step propagates the tree extension in every iteration as described in the previous sections. However, not only it yields the path solution if any found, but it also provides the two conditions, PathFound and StartExploitation, that determine whether the exploitation on the current solutions should start. The condition of PathFound is simply a boolean parameter to indicate that the exploration step has found a new path. On the other hand, StartExploitation represents the maturity of the conditions for exploitation to take place for path optimization. Various strategies can be followed to decide when to start the exploitation step. The simplest strategy would be to utilize it every time a new path found, which might not be an efficient approach, though.

If the conditions for the exploitation are met, in Line 4, two steps define the path optimization. In the first step, from potentially the multiple solutions found so far, a path that should be optimized has to be selected. Again, this selection can be done according to numerous strategies. One way is always to select the best path with the lowest cost, which may eliminate some of the candidates that can potentially yield the best solution. Another strategy would be to develop a comparison metric that can approximately quantify how much a path can be optimized more such that the maximum gain from the path optimization can be achieved by the selection of the highest rewarding path comparing the multiple solutions. In the second step, rewiring operation of the RRT* algorithm is utilized for a fixed number of iteration so that in each iteration it locally optimizes the path segments and by so at the end of the iterations global optimization is asymptotically achieved. In this algorithm, the local rewiring operations can follow a randomized approach by the selection of random nodes along to path and the random configuration nodes generated near the selected nodes to utilize the local optimizations among these nodes.

CHAPTER 4

DERIVATION OF UTILITY (COST) FUNCTIONAL FOR THE PATH PLANNING OF STAARS OPERATIONS

The utility approach is a common practice that is studied in various multi-objective optimization problems. The main difference between the cost and utility approaches, which both are common in path planning problems, is that the optimization requires the minimization of strictly the negative attribute in the former approach, whereas the latter one uses the maximization techniques on a more general attribute set. In essence, the utility theory provides more flexible approaches in general.

In this chapter, a generic utility functional that will be utilized by the path planner as an inverse cost function to quantify the goodness of the path segments and the paths found is derived. The derived functional is used during the extension of the tree branches and the optimization of the local path segments. Basically, anytime when a decision requires the quality of the node extension or the comparison between different path segments or paths, the quantification is being made by this utility functional.

The proposed utility approach is essentially the critical part where all the components of the risk assessment framework from the previous chapters are embedded in a generic formulation with high-level terms that will also consider the mission objectives, benefits or advantages of the UAS operations along with the risks incurred by these operations. Therefore, both positive and negative aspects of the UAS operations are taken into account during the path planning by this approach.

The derivation of the proposed utility functional is described in two steps. In the first step, the derivation of the path utility function in a path integral form, which will be used by the path planner, is explained by using point (node) utilities that is similar to the derivation of the risk function. In the second step, the structure of the point utilities and the mathematical formulation to construct them are explained.

4.1 Path Utility Function

Path utility is defined as the cumulative utility obtained along the trajectory of a UAS mission and is formulated with a path integral in Equation (4.1).

$$\mathcal{U}(\tau_{0..T}) = \int_0^T P(Success|\tau_{0..t})\lambda_{\mathcal{U}}(\tau_t|\tau_{0..t})\,dt \tag{4.1}$$

The path integral is composed of two key factors. The first one is the success probability of the platform to reach the current point τ_t along its planned trajectory $\tau_{0..t}$, and the other factor is the expected rate of reward/payoff, $\lambda_{\mathcal{U}}$, at the point given the current trajectory. In this integration, the first term plays the role of a weighting factor for the utility contributions of the point to the cumulative path utility based on the likelihood that this point will actually be reached along the trajectory. This weighting also implicitly states that if the vehicle does not succeed to reach a point, either due to a catastrophic failure or the termination of the mission, the utilities of the rest of the trajectory should not be considered in the path utility.

The success probability of the platform depends on numerous factors in a real UAS scenario which can be analyzed using many different approaches. In this work, a general terminology is used as the events that can happen on or around the platform, and once happened, can impact the success of the platform. These events are categorized as catastrophic events and non-catastrophic events. In the case of a catastrophic

event, the platform undergoes an uncontrollable regime, resulting in the termination of the mission with a potential impact to the ground. In a non-catastrophic event, on the other hand, the platform is assumed to be controllable and can still continue its mission. While other events, such as partially controllable failures can occur in the real world and can be integrated into the framework, we will here concentrate on only these two event types, resulting in the situation where only the catastrophic events can impact the success of the platform by causing its complete failure. Under this assumption, the success probability of the platform to reach the current trajectory point is equal to the probability of not having encountered any catastrophic failures, F_c, until this point. Using this fact, (4.1) becomes (4.2)

$$\mathcal{U}(\tau_{0..T}) = \int_0^T P(\neg F_c|\tau_{0..t})\lambda_{\mathcal{U}}(\tau_t|\tau_{0..t})\, dt \tag{4.2}$$

The reward rate $\lambda_{\mathcal{U}}$ represents the expected incremental utility contribution of the events happening at trajectory location τ_t, and can be defined for the two categories of events considered here, which are events that can only happen once or that can happen multiple times over the trajectory. For the former category, the underlying reward from an event can be obtained only at a given point and on following occurrences to the same point, the same event does no longer contribute to the path utility. This type of events may model the utility of reaching an intermediate goal location, or having a permanent component failure. The reward rate, $\lambda_{\mathcal{U}}$, for these one-time events can be expressed as follows:

$$\lambda_{\mathcal{U}}(\tau_t|\tau_{0..t}) = \sum_{i \in Events} P(\neg e_i|\tau_{0..t})\lambda_{e_i}(\tau_t|\tau_{0..t})\mathcal{U}_i(\tau_t|\tau_{0..t})w_i \tag{4.3}$$

where τ_t is the trajectory node at which the event e_i happens, and w_i is the relative weighting factor of the utility contribution of the i^{th} event at the same node. It is

important to note here that for catastrophic events, the term $P(\neg e_i|\tau_{0..t})$ moves out of the sum and becomes part of the probability that the trajectory is still active, $P(\neg F_c|\tau_{0..t})$, in Equation (4.2) since occurrence of a catastrophic event terminates any future utility of any other event.

The reward rate for events that may happen multiple times at a trajectory location is modeled with a rate parameter of the event, defined in unit time, as below. Non-critical, temporary platform or component failure events, as well as general costs incurred along the trajectory, can be modeled by this approach.

$$\lambda_{\mathcal{U}}(\tau_t|\tau_{0..t}) = \sum_{i \in Events} \lambda_{e_i}(\tau_t|\tau_{0..t})\mathcal{U}_i(\tau_t|\tau_{0..t})w_i \tag{4.4}$$

where $\lambda_{e_i}(\tau_t|\tau_{0..t})$ is the expected number of times per time unit that event e_i is happening at point τ_t given the trajectory.

In the case of events that are guaranteed to occur at a particular point along the trajectory such as, for example, the reaching of a delivery location or events caused directly by control actions, the event rate, $\lambda_{e_i}(\tau_t|\tau_{0..t})$, can be expressed (with a slight abuse of notation) by a Dirac delta function as $\lambda_{e_i}(\tau_t|\tau_{0..t}) = \delta(\tau_t - \tau_{t_{e_i}}|\tau_{0..t})$. This allows the incorporation of mission goals associated with specific actions or locations.

For a mission having a mixture of these events, the expected reward rate term in (4.2) becomes the sum of (4.3) and (4.4) with corresponding events.

With this approach, it is proposed to facilitate a task-level decision-making capability through the maximization of a carefully constructed path utility function that includes possible task-centric events and utility components such as reaching a destination, accomplishing a task component, violating safety or regulatory considerations, or failure of the platform. According to the objectives of an assigned task and the other considerations like ground safety, the proposed utility approach allows

to consider and generate solutions other than purely completing the mission. An example for this could be a "stay on the ground" decision of a UAS, which might yield the highest utility, for a package delivery mission in adversarial weather conditions. With its bare interpretation, in the proposed framework, the final decision is to choose the highest utility path which can be extended to highly complex scenarios with a detailed analysis of the events that can happen during a UAS mission.

4.2 Calculation of Point Utilities

Rewards/Utility changes obtained at a specific point are calculated according to the events happening on the platform that affect the ground or the mission parameters. These events are defined to capture the mission objectives and the safety concerns. For an illustration, the event of taking aerial pictures of an area at a trajectory point has an effect on the mission and on the ground, which yields the utility of that point. In this case, for example, taking pictures yields a benefit in terms of obtaining the pictures but also incurs a cost in terms of the potential invasion of privacy of persons on the ground. Another example is that the event of a catastrophic failure on the platform at a trajectory point has also an impact on the ground in terms of potential injury and property damage caused by the impact on the ground with an associated utility.

Calculation of the node utility can be divided in two stages. The first stage is to find the available utility at a location on the ground given the previous trajectory and the point at which the event happened. In the second stage, the utilities for ground locations are integrated over the attainable area impacted by the event.

The first stage of the calculation is shown in Equation (4.5). This term is the spatial map of the utility for the given event.

$$\mathcal{U}_{i,\tau,t}(\mathcal{X}) = \int_{A_{eff}} \mathcal{M}(x|\tau_{0..t}, \tau_{t_{e_i}}, \mathcal{X})\, dx \tag{4.5}$$

Here $\mathcal{X}$ is the location on the ground where the utility is computed, and A_{eff} is the effective area that the utility calculation at $\mathcal{X}$ depends on. In case of an impact scenario, this area can be approximated by the lethal area affected by the UAS platform impact at a location $\mathcal{X}$. $\mathcal{M}$ is the spatial mapping (distribution) of the available utility resulted from the event e_i. Also, the notation for the utility of the location $\mathcal{X}$ is selected as $\mathcal{U}_{i,\tau,t}(\mathcal{X}) = \mathcal{U}_i(\mathcal{X}|\tau_{0..t}, \tau_t = \tau_{t_{e_i}})$.

In the second stage of the point utility calculation, the expected point utility is computed by the integration of the location-dependent utilities on the ground weighed by the probability distribution of the attainability of ground locations for an event e_i happening at the current trajectory point, where the integration is carried out over the attainable area A_{e_i}:

$$\mathcal{U}_i(\tau_t|\tau_{0..t}) = \int_{A_{e_i}} p(\mathcal{X}|\tau_{0..t}, \tau_{t_{e_i}}) \mathcal{U}_{i,\tau,t}(\mathcal{X})\, d\mathcal{X} \tag{4.6}$$

$p(\mathcal{X}|\tau_{0..t}, \tau_{t_{e_i}})$ here is the probability distribution of attainability of the locations, $\mathcal{X}$, on the ground for an event happening at the current trajectory point, and it represents the likelihood of obtaining the underlying utility at each location. It is important to note here that the attainability of a ground location concept is used in a wide sense here. For some events such as catastrophic failures, it can be defined as the impact probability at a location, or for the event of taking aerial pictures of an area, it could be represented as the success probability of covering a location on the ground in the picture.

The steps for the construction of (4.5) and the integration of (4.6) is described in more detail in [30] for the risk of exposure of the ground to the failing UAS platform. In this previous work it was assumed that the previous trajectory does not affect

the risk of the current point and the underlying risk exposure distribution is static. Under this assumption, the risk associated with the trajectory point where the failure happened is given in the equation below:

$$R_F(\tau_t) = \int_{A_F} p(\mathcal{X}_{imp}|\tau_t = \tau_{t_F}) \Big[\int_{A_{UAS}} PREM(u|\mathcal{X}_{imp})\, du \Big]\, d\mathcal{X}_{imp} \tag{4.7}$$

where the first term in the integral is the UAS impact location distribution on the ground given the trajectory node of failure and the second term computes the value of total risk exposures given the impacted location by the integral of the distribution of the risk of exposure on the ground, $PREM$, over the effected region approximated by the vehicle area, A_{UAS}.

Note that the formulation of proposed utility function is flexible enough to accommodate most commonly used cost functions in path planning such as distance traveled or total time by treating them as an event happening every instance of time and assigning an appropriate utility. To illustrate this, time can be included using Equation (4.4) by setting the first term (the event rate) to 1 and the utility term to -1, which integrates to the elapsed time along the trajectory as a negative utility component. Similarly, for the distance traveled case, one can assign the negative speed of the vehicle as the reward rate at a point to account for total distance traveled in the utility optimization of the path.

CHAPTER 5

SIMULATION OF SIMPLE STAARS SCENARIOS

In this chapter, the simple UAS scenarios will be demonstrated using the proposed risk assessment framework and the utility-based path planning approach introduced in the previous chapters. Before getting into the scenario descriptions and the results, the simulation environment section summarizes the assumptions made for the scenario implementations including the PREM construction from the Geographical Information System (GIS) database as a priori data, the utility formulations for the path planning of UAS scenarios according to the assumptions and the path planning algorithm to be used in the simulations.

5.1 Simulation Environment

In the simulation scenarios of this thesis, the construction of the PREM, as formulated in Equation (2.3), is explained only for impact-related risk exposures. Exposure of buildings to the UAS is modeled within the PREM concept using the building footprints in a specific area, taken from geographical information system (GIS) database. By the help of aerial and satellite imagery, building footprint data are often uploaded to the GIS database by various efforts, [31], where the footprints are represented by the polygonal shapes using the corner locations of each building. Using these polygonal shapes, the distribution of the risk exposure is modeled by the mixture of Gaussian probability density functions (PDFs) such that the mean of each PDF represents the concentration point (center location) of the risk exposure and the standard deviation of the PDF represents how far the exposure spreads out

(covariance, i.e. modeling parameter). The center location of each PDF is chosen to be the centroid of corresponding polygon and the covariance is computed from the corner points and the center location. The construction of PREM with a weighted sum of Gaussian PDFs is shown in Equation (5.1).

$$PREM = \sum_{j=1}^{\text{Num. of PDF}} \pi(S_j)\, \mathcal{N}(\mu_j, \sigma_j) \tag{5.1}$$

where S_j is the individual buildings (PDFs), $\mu_j = [l_{x_j} \;\; l_{y_j}]^T$ and $\mathcal{N}(\mu_j, \sigma_j)$ is the bivariate normal distribution. Also, π represents the relative weights of each S_j with the condition of $\sum_j \pi(S_j) = 1$. Relative weights of the building footprints are assumed to be related with the individual polygonal area and the total area, and modeled as the fractions ($\pi(S_j) = \text{Area}(S_j) / \sum_j \text{Area}(S_j)$).

For the demonstration of the proposed risk assessment framework with the utility-based path planning approach, the path utility function is constructed for the simple UAS package delivery scenarios where the events that can happen during the mission are catastrophic failure events, delivering the package to the designated location, landing on another warehouse/station to leave the package there or to land/stay at the take-off location. In these scenarios, the catastrophic events on the vehicle are modeled as Poisson processes having constant failure rates using (4.4) and the other events as the single node events using (4.3). Node utilities for the corresponding events are presumed to depend only on the location of the current node and the underlying utility rate is independent of time or the previous trajectory. With these assumptions, the path utility function becomes as follows:

$$\mathcal{U}(\tau_{0..T}) = \int_0^T e^{-\lambda t} \lambda_{\mathcal{U}}(\tau_t)\, dt \tag{5.2}$$

One advantage of using Poisson process failure models is their independent and stationary memoryless properties. Although time is known for each node on the forward tree during extension, time of the nodes on the backward trees is relative to the unknown end time and it runs backward in time. Using the independent and stationary increments of the Poisson process, the relative increments of the path utilities can be computed over the backward trajectories and the complete path utility can be found when connecting the forward to the backward branch using a simple operation. This also allows us to use rewiring operations efficiently on the backward trees.

It can also be noticed from Equation (5.2) that the utilities are not simply additive along the path. Instead, the exponential factor in the first term, $(e^{-\lambda t})$ as a success probability of the next path segment, implies the exponential relation between the consecutive node utilities during the integration.

Path utility propagation for the backward tree is formulated in (5.3). Trajectory nodes on a backward tree are given as $(\tau_T, ..., \tau_{t_{k+1}}, \tau_{t_k}, ...)$ starting from a goal node τ_T in backward order.

$$\mathcal{U}(\tau_{T..t_k}) = \int_{t_k}^{t_{k+1}} e^{-\lambda(t-t_k)} \lambda_{\mathcal{U}}(\tau_t) dt + e^{-\lambda \Delta t_k} \mathcal{U}(\tau_{T..t_{k+1}}) \tag{5.3}$$

where $\Delta t_k = t_{k+1} - t_k$ is the time increment while extending a backward branch. In this function, the integral term assumes that time starts from node τ_{t_k} and it computes the incremental utility of the path segment $(\tau_{t_k}, \tau_{t_{k+1}})$. The second term in the function adds the cumulative incremental utilities until the previous node $\tau_{t_{k+1}}$ by multiplying them with the incremental success probability during this extension.

Using the above functions, total path utility calculation when both trees are connected is given below.

$$\mathcal{U}(\tau_{0..T}) = \mathcal{U}(\tau_{0..t}) + e^{-\lambda t}\mathcal{U}(\tau_{T..t}) \tag{5.4}$$

Assuming both trees are connected at node τ_t, the first term computes the path utility accumulated by the forward tree extension until the connection, and the second term propagates the time on the backward tree nodes by adding the connection time t and the resulting utility accumulation over the backward tree, discounted by the likelihood that the connection point is reached.

5.1.1 Implementation Details

In the proposed utility-based approach to the path and task planning problem of UAS operations, a modified multi-tree variant of T-RRT* algorithms [28, 25, 29] is used as an optimization technique to maximize the proposed path utility function over the planned trajectories. The planning algorithm grows a forward tree and multiple backward trees (one from each potential goal - i.e. allowed path end location) by iteratively sampling from the configuration space as explained in Chapter 3. The sampling uses the goal bias, transition test and PREM guided sample generation heuristics to drive the extension of trees faster to the goal configurations and also to efficiently explore the high utility regions first. The pseudo-code of the algorithm is given in Algorithm 9.

Provided with initial and goal configurations, goal connection biases of the forward and backward trees, and the connection threshold, the algorithm starts with initializing the forward tree T_{fw} from the initial configuration x_{init} and the backward trees T_{bw} from the goal configurations $\mathcal{X}_{goal}$, setting the path parameters to the empty set. In an iterative loop, first, the forward tree extends a branch towards a random

Algorithm 9 Multi-T-RRT*

Input: $x_{init}, \mathcal{X}_{goal}, P_{goal}, P_{connect}, \mathcal{C}, thrs$

Output: $E_{path}, \mathcal{U}_{path}, \sigma_{path}, T_{fwd}, T_{bwd}$

Initialize($x_{init}, \mathcal{X}_{goal}, T_{fw}, T_{bw}, E_{path}, \mathcal{U}_{path}, \sigma_{path}$)

for $i = 1$ to $iterMax$ **do**
  $q_{rand} \leftarrow ChooseTarget(\mathcal{X}_{goal}, P_{goal}, \mathcal{C})$
  $T_{fw} \leftarrow Extend\&Rewire\_Fwd(q_{rand}, T_{fw})$
  $[S, N_{IDs}, T_{IDs}] \leftarrow ConnectTrees(T_{fw}, T_{bw}, thrs)$
  if $S = True$ **then**
    $[E, \mathcal{U}, \sigma] \leftarrow CreatePath(N_{IDs}, T_{IDs}, T_{fw}, T_{bw})$
    if $\mathcal{U} > \mathcal{U}_{path}$ **then**
      $[E_{path}, \mathcal{U}_{path}, \sigma_{path}] \leftarrow [E, \mathcal{U}, \sigma]$
    end if
  end if
  $Q_{rand} \leftarrow ChooseTarget([x_{init}, q_{rand}], P_{connect}, \mathcal{C})$
  $T_{bw} \leftarrow Extend\&Rewire\_Bwd(Q_{rand}, T_{bw})$
  $[S, N_{IDs}, T_{IDs}] \leftarrow ConnectTrees(T_{fw}, T_{bw}, thrs)$
  if $S = True$ **then**
    $[E, \mathcal{U}, \sigma] \leftarrow CreatePath(N_{IDs}, T_{IDs}, T_{fw}, T_{bw})$
    if $\mathcal{U} > \mathcal{U}_{path}$ **then**
      $[E_{path}, \mathcal{U}_{path}, \sigma_{path}] \leftarrow [E, \mathcal{U}, \sigma]$
    end if
  end if
end for
return $E_{path}, \mathcal{U}_{path}, \sigma_{path}, T_{fw}, T_{bw}$

configuration chosen from the $\mathcal{C}$ space according to the goal bias and PREM guided sampling heuristics, if the extension passes the transition test shown in Algorithm 10.

Algorithm 10 *Extend&Rewire_Fwd*

Input: q_{rand}, T_{fw}

Output: T_{fwd}

1: $q_{nearest} \leftarrow NearestNode(q_{rand}, T_{fw})$

2: $q_{new} \leftarrow steer(q_{rand}, q_{nearest})$

3: $\mathcal{U}(q_{new}) \leftarrow NodeUtility(q_{new})$

4: **if** $TransitionTest(T_{fw}, \mathcal{U}(q_{new}), \mathcal{U}(q_{nearest}))$ **then**

5: $\quad \mathcal{U}(\sigma_{new}) \leftarrow PathUtility\_Fwd(q_{new}, \sigma_{nearest})$

6: $\quad addNode(T_{fw}, [q_{new}, q_{nearest}], \mathcal{U}(q_{new}), \mathcal{U}(\sigma_{new}))$

7: $\quad Q_{near} \leftarrow NearNeighbors(T_{fw}, q_{new})$

8: $\quad T_{fw} \leftarrow Rewire\_Fwd(q_{new}, Q_{near}, T_{fw})$

9: **end if**

10: **return** T_{fw}

If the extension is successful, the extended node and the edge are added to the tree with its accumulated link utility. After that, the near neighbor search function finds the neighbor nodes around q_{new} within a distance as in the RRT* algorithm [28]. The rewiring operation is performed between the near neighbors, Q_{near}, and the extended node q_{new}, and the tree is maintained.

It should be noted here that some of the functions denoted with $\_Fwd$ or $\_Bwd$ are designated specifically for the forward or backward trees. The reason is that since the path utility function developed in Equation (4.2) depends on the trajectory from root node τ_0 to current node and the backward trees have no information about the

Algorithm 11 *CreatePath*

Input: $N_{IDs}, T_{IDs}, T_{fw}, T_{bw}$

Output: $E_{path}, \mathcal{U}_{path}, \sigma_{path}$

1: $T_{back} \leftarrow IdentifyBackwardTree(T_{IDs}, T_{bw})$

2: $[E, \mathcal{U}, \sigma]_{path} \leftarrow biBackTrack(T_{fw}, T_{back}, N_{IDs})$

3: **return** $E_{path}, \mathcal{U}_{path}, \sigma_{path}$

forward trajectory until they are connected, the calculation and the accumulation of path utilities are different for the forward and backward trees.

The *ConnectTrees* function checks the possible connections between the forward tree and the backward trees, and if there are any, it returns with the IDs of the connected nodes and their corresponding tree identifiers, and with a boolean indicating the connection success. If the connection is successful, a path is created by backtracking from the connection nodes on the forward tree through the connected backward tree. According to the calculated utility of the path created, if it surpasses the best path found so far, the best path and its utility are updated to the new one.

The extension, rewiring, and the connection check processes are repeated for the backward trees individually in the same iteration, except with a slightly changed path utility calculation as mentioned above. If any higher utility path is found during the extension of the backward trees, the best path is again updated, and the whole iteration is repeated until the termination condition (in this case a maximum iteration count) is reached.

The scenarios include four independent catastrophic failure events, denoted with F_1, F_2, F_3 and F_4 with the constant failure occurrence rates, λ, and elliptical impact domains represented by the major and minor axis, listed in Table 5.1.

Table 5.1: Failure Mode Parameters

Failure Modes	Failure Rates	Impact Domain Shape	Orientation
F_1	10^{-5} per hour	Ellipse (50 m x 33 m)	$\angle$ 0°
F_2	10^{-4} per hour	Ellipse (37 m x 21 m)	$\angle$ -30°
F_3	10^{-3} per hour	Ellipse (33 m x 16 m)	$\angle$ 0°
F_4	10^{-4} per hour	Ellipse (37 m x 21 m)	$\angle$ 30°

Although it may not be the actual case, to demonstrate the concepts, the ground impact location distributions of the failure events are assumed to follow the truncated bivariate normal distributions where the covariance vectors are found to make the effective region of the impact distributions (3σ) fits inside the corresponding elliptical regions. In addition, the mean of the distribution is shifted along the major axis by the quarter length to accommodate the inertial effect of the motion on the impact locations. Figure 5.1 shows the elliptical impact regions and the weighted sum of the impact location distributions according to the Equation (2.5).

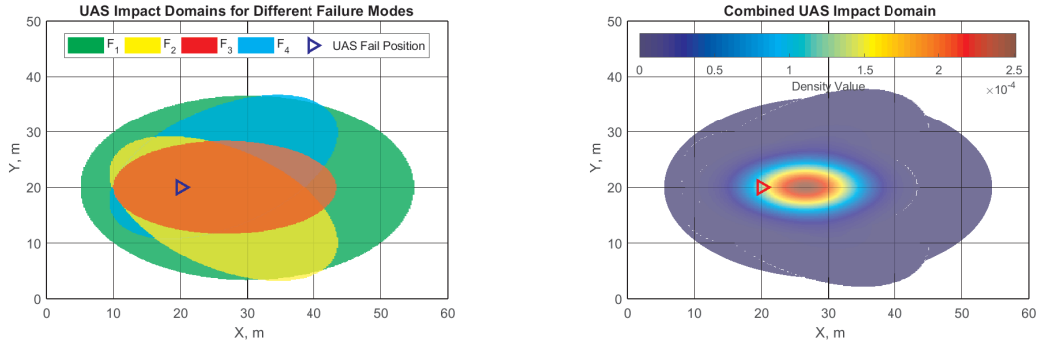

(a) Impact domains of failure modes - separately

(b) Combined ground impact probability distribution

Figure 5.1: Failure mode impact domains and combined ground impact probability distribution

As mentioned before, these assumptions are arbitrarily selected. However, given a more detailed and accurate analysis of the ground impact distributions for individual

failure events, the proposed approach can easily be adapted to represent more realistic scenarios.

Parameters required for the path planning algorithm are listed in Table 5.2 for all scenarios. The maximum iteration number for the run is determined to be 15000. However, the longer the runtime is, the more optimized solution can be obtained due to asymptotical optimality of the RRT* algorithms. The speed of the vehicle is chosen to be 40 km/h with a maximum step size of 12 meters. Goal bias of 0.01 for exploring the regions near the goal position and the connection bias of 0.02 for connecting backward trees to the forward tree are used.

Table 5.2: RRT Parameters for Simulations

V	40 km/h	**Step Size**	12 m	P_{goal}	0.01
IterMax	15000	**Threshold**	0.2× StepSize	$P_{connect}$	0.02

5.2 Scenarios

Two different UAS package delivery scenarios are demonstrated in this section. In the first scenario, instead of a utility-based approach, the risk function, introduced in Equation (2.14), is employed to find the least risky path between the initial and goal positions considering. Therefore, the decision criteria in this scenario do not consider any other mission objectives, except for the accumulated risk values. On the other hand, the second scenario uses the multi-objective decision criteria, which is introduced in Chapter 4 by the utility-based path planning approach. The second scenario considers the profits of accomplishing mission objectives as well as the risks incurred by the UAS operation during the path planning and decision-making processes.

5.2.1 Scenario 1

In this scenario, a small residential area with a rectangular dimension of 400 by 400 meters is selected as the UAS operation area in Fort Worth, TX. For this region, PREM is constructed for the risk of flying over properties and traffic, which is assumed to be stationary. Therefore, the risk of being hit by the UAS for the properties and the vehicles will be considered by the risk assessment framework. Two cases are investigated in this scenario to compare the results. In the first case, shown in Figure 5.2(a), only the property risk exposure is present in the environment (late night UAS operation). In Figure 5.2(b), the second case includes both property and traffic risk exposures for the risk assessment (daytime UAS operation). The weights that are used to construct PREM from the combination of both layers are 0.4 and 0.6 respectively. Note that, the selection of weights on different layers plays an important role in path characteristics and task-awareness, and therefore, they should be extensively investigated, which is outside the scope of this thesis. A higher weight on the risk of flying over traffic might be more realistic in real-life due to the potential cause of catastrophic secondary incidents. Nevertheless, different cases will be demonstrated for diversity and comparison.

For the selection of start and goal positions, although they can be any two random positions, they are selected to show the effect of various PREMs on the generated paths. Finally, the path planner algorithm is run to find a near-optimal path while continuously exploring the whole map and optimizing the previously found paths simultaneously.

Results of the path planning for both cases are shown in Figures 5.3-5.4, where the solid red lines in Figures 5.3(a)-5.4(a) are the final paths for the first and second cases after 15000 iterations, whereas, the blue dashed lines are the paths found during the previous iterations.

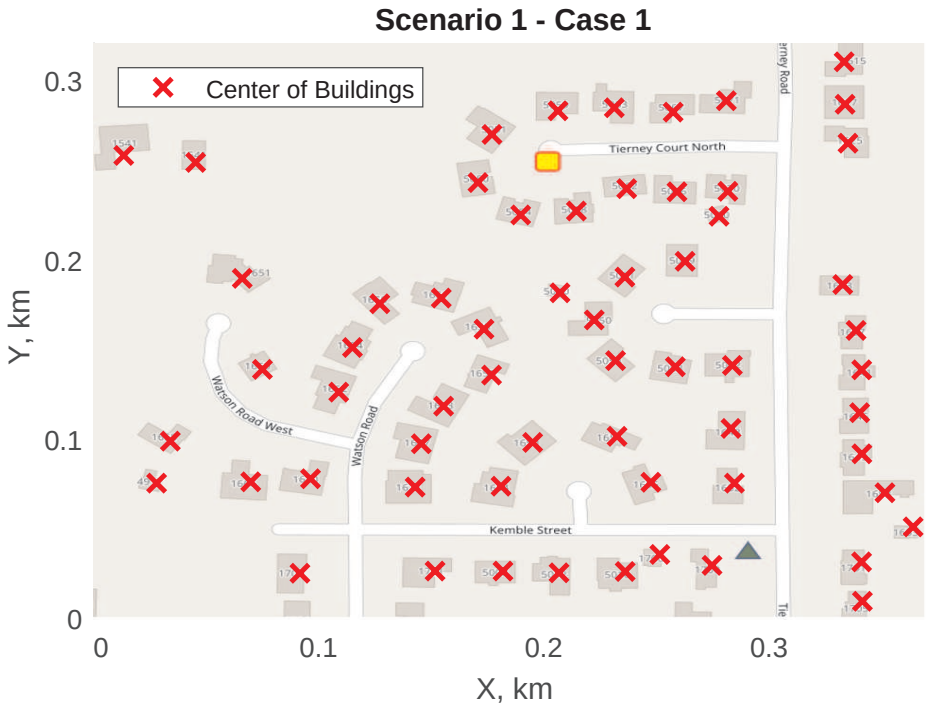

(a) 1st Scenario Map - Case 1

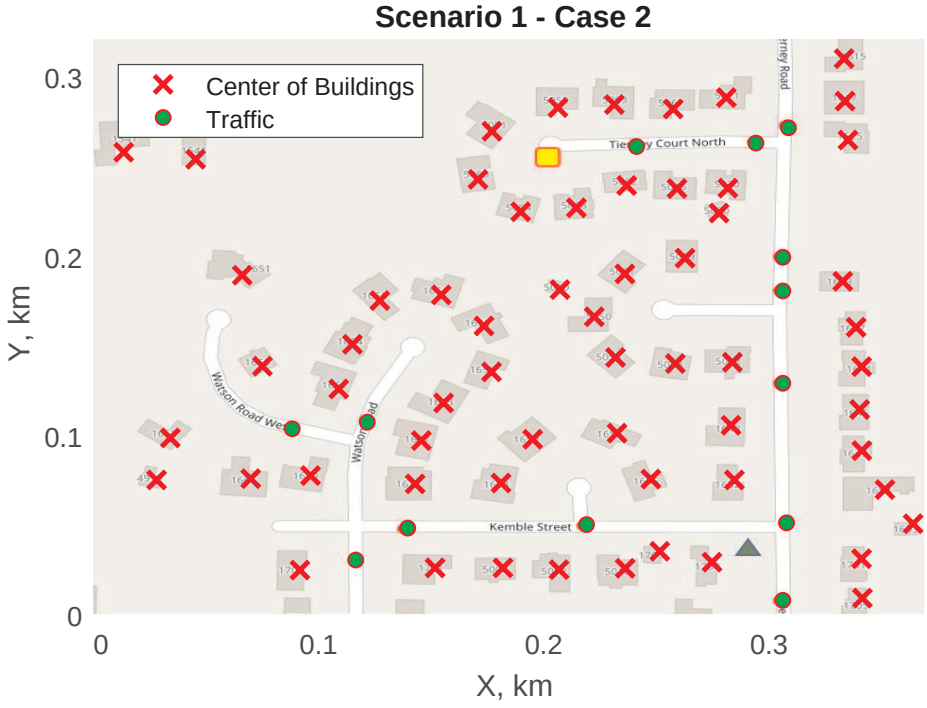

(b) 1st Scenario Map - Case 2

Figure 5.2: Case maps for Scenario 1

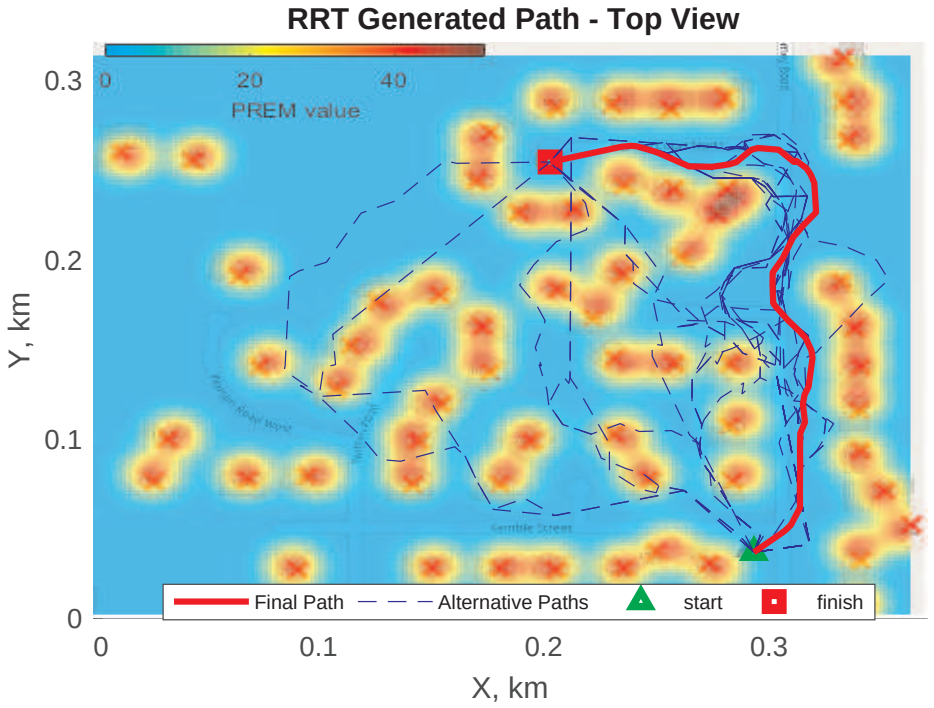

(a) RRT Generated Paths - Case 1

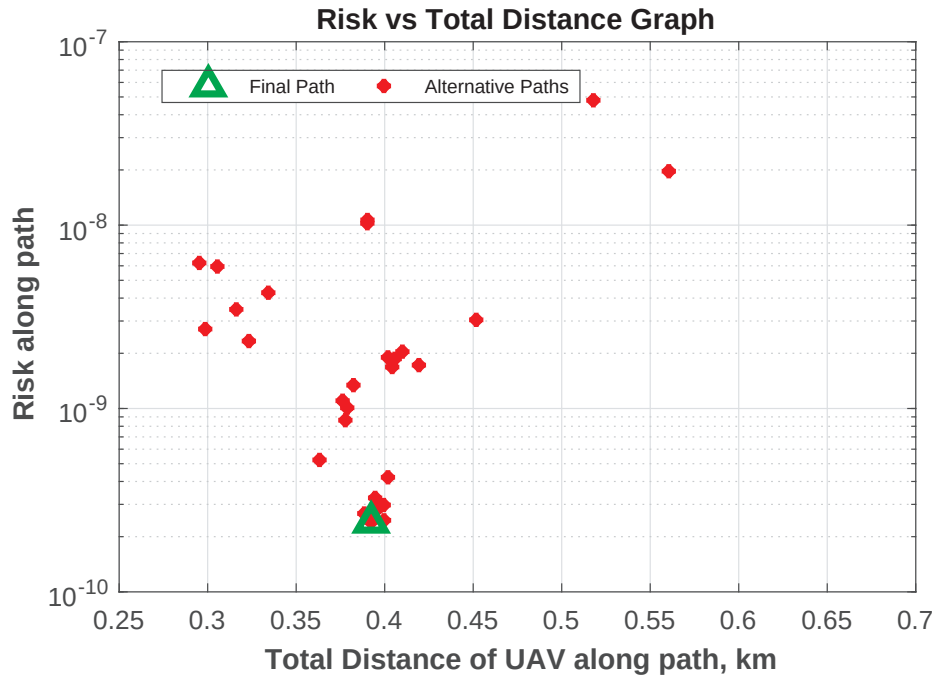

(b) Risk Levels vs Total Distance Chart - Case 1

Figure 5.3: Results of the path planning for Scenario 1 - Case 1

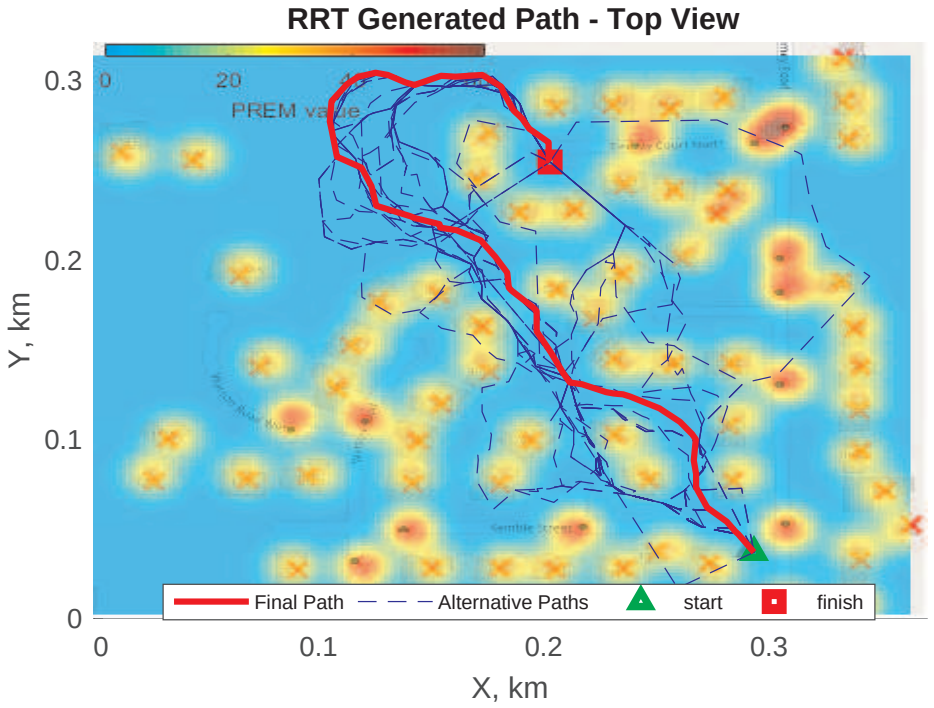

(a) RRT Generated Paths - Case 2

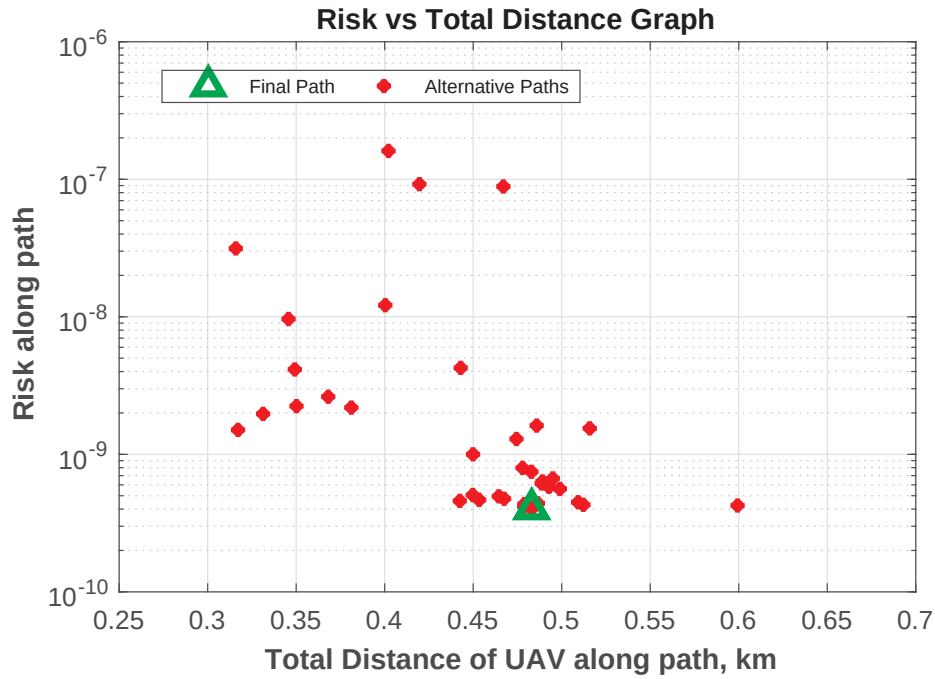

(b) Risk Levels vs Total Distance Chart - Case 2

Figure 5.4: Results of the path planning for Scenario 1 - Case 2

In the first case, since there is no traffic present on the map, reaching the goal position by traveling over the streets gives the lowest risk path as expected. However, in the second case, having a traffic activity on the streets changes the underlying risk exposure map, and it drives planner algorithm to look for the alternative paths to minimize the total risk until reaching the goal. Comparing with the first case, the gaps between buildings, without street intersections, and the property backyards give the lowest risk path in the second case as seen in Figure 5.4(a). This means that flying over traffic accumulates a higher risk in total than flying near the buildings, as it was intended in PREM construction. Moreover, it is worth noting that the regions that potentially accumulate low risks depend on the selection of ground impact location distributions too. Therefore, those regions can widely vary according to those selections. For instance, a constant wind flow from one direction over the region would shift the ground impact regions in the same direction, and it might result in having the lowest risk path that goes above the properties. Thus, path characteristics for the missions depend on both the underlying risk exposures (PREM) and the vehicle's failure mode outcomes including the environmental effects.

Plots in Figures 5.3(b)-5.4(b) show the paths found during the path planning iterations with respect to their risk levels and the total distance traveled. Note that these charts can be used to determine whether the mission is in acceptable risk limits or within the vehicle's range if the limits are known. In addition, the information about the environment, underlying high-risk regions, and potential paths can be inferred from these charts during the planning process. For example, the convergence rate of the planning can be learned and used to make the decisions for concluding the search, or even, for ruling out some of the map regions.

Finally, as it can be noticed from the path solutions that some of the very first paths have long straight edges, which indicates that the RRT has not fully explored

those regions yet. As the process advances, those straight lines are optimized on the tree by the rewiring operations to minimize the total risk along the path, and they usually turn out to be the smoother curly path segments which yield the low-risk levels due to the selection of the risk exposure representations.

5.2.2 Scenario 2

In this scenario, another small region is selected in Dallas, TX, to demonstrate the proposed utility-based multi-objective optimization approach considering the developed risk assessment framework and the selected mission objectives. The region is shown in Figure 5.5.

Figure 5.5: UAS package delivery map - Scenario 2

The mission is to deliver a package from a start location to a goal location with a highest possible path utility. The mission objectives are to deliver the package to the original destination with a minimum intrusion (risk) to the properties and, if the utility of delivering to this location is lower than the expected utility of the other (alternate) delivery locations, then, to consider delivering to the other locations, or do not to take-off at all. In this sense, the proposed system not only plans a path but also makes task-level decisions between different delivery locations and whether to deliver at all. These decisions are being made according to the comparison between the utility values of the mission objectives. The utilities are composed of the benefits obtained by completing the mission objectives as positive utility and the risk accumulated during the mission as a negative utility.

In this scenario, the other package drop locations are shown on the map, and the utility of package delivery to these locations are determined according to their distance to the original drop location, where the numbers on the scenario map indicate the closeness of these locations to the goal. Point utility values of the mission objectives for all possible drop locations are selected as $10 \cdot 10^{-9}, 4 \cdot 10^{-9}, 3 \cdot 10^{-9}$ and $1 \cdot 10^{-9}$, respectively. In addition, 0 utility value is assigned to the "Do-Not-Fly" action which means no benefit is obtained. Note that in a real scenario, this might be a loss with a negative utility.

The scenario has the same failure events as in the first scenario, except that the failure occurrence rates, λ, are chosen for two different cases where the first case represents the normal operating conditions with average failure rates and the second case stands for the condition with increased failure occurrences with the same impact regions. Table 5.3 lists the failure rates for both cases.

The aim is to show the effect of operating conditions on the task-level decision and the path characteristics.

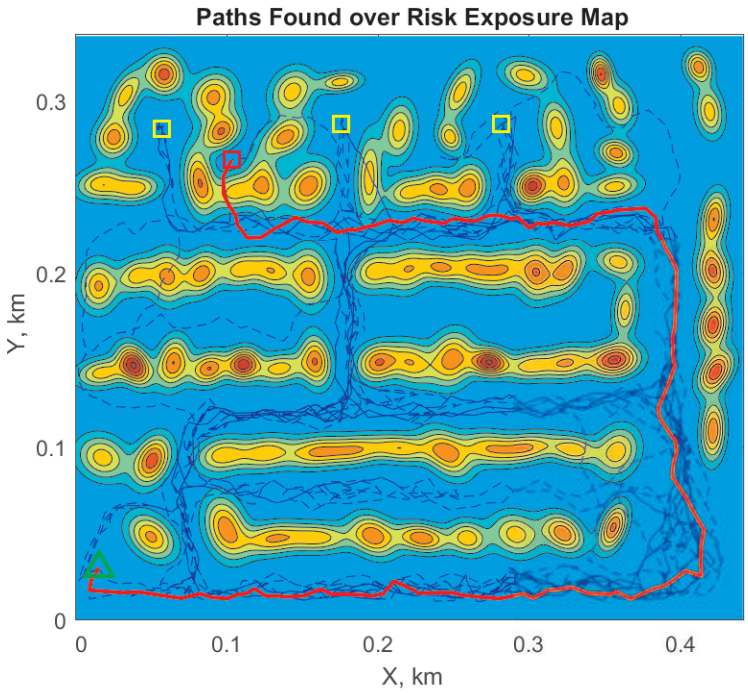

(a) Paths found are shown over $PREM$ - Case 1

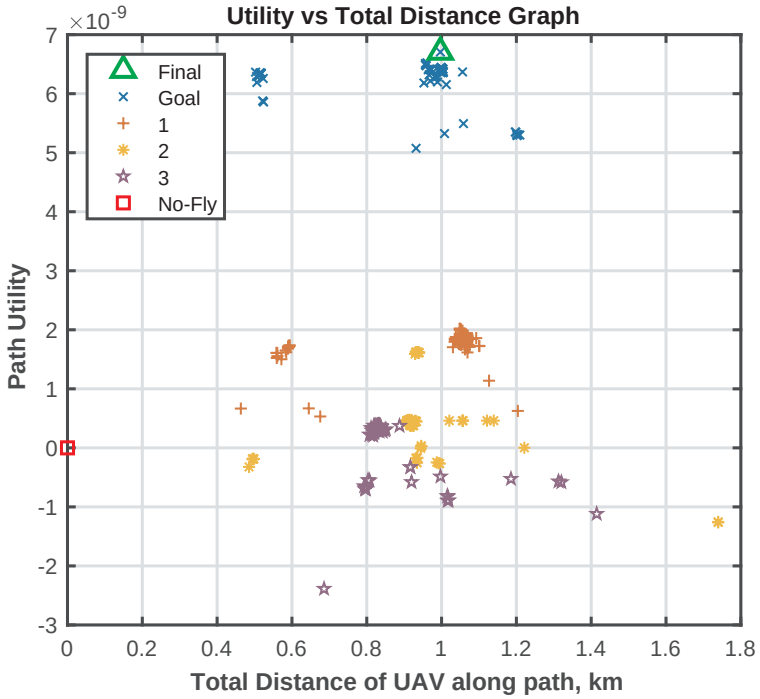

(b) Utility vs Total Length of the Paths - Case 1

Figure 5.6: Results of the path planning for Scenario 2 - Case 1

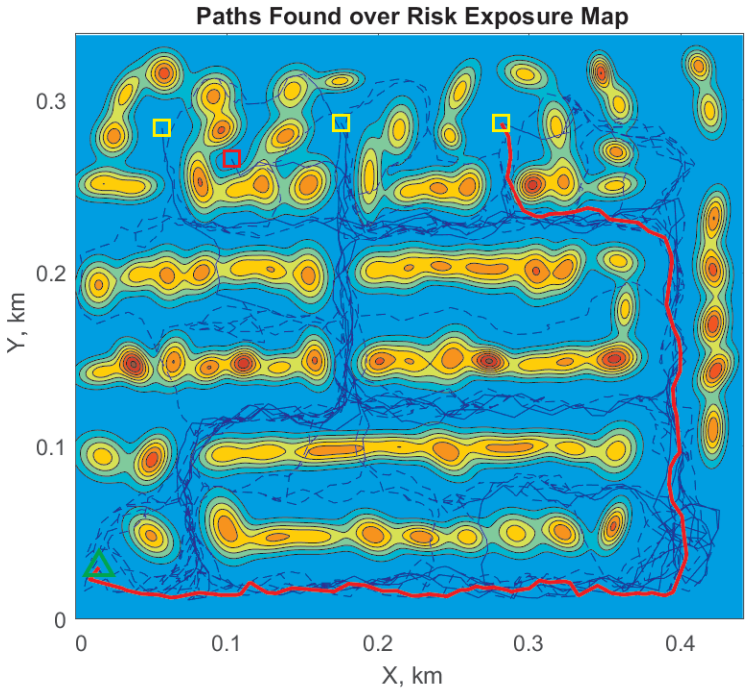

(a) Paths found are shown over $PREM$ - Case 2

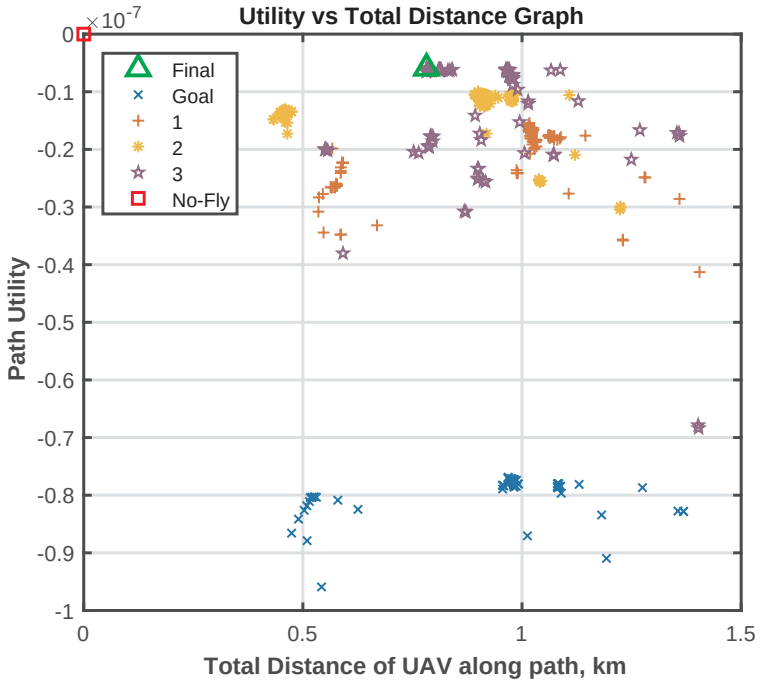

(b) Utility vs Total Length of the Paths - Case 2

Figure 5.7: Results of the path planning for Scenario 2 - Case 2

Table 5.3: Catastrophic Failure Event Rates for Scenario 2

1/hr	F_1	F_2	F_3	F_4
Case 1	0.001	0.05	0.01	0.05
Case 2	0.01	0.5	0.1	0.5

Paths that are found during the optimization of the proposed utility function are plotted over the risk exposure map of the area in Figures 5.6(a)-5.7(a) for the selected cases. In these plots, the solid red line is the final path maximizing the utility, while the dashed blue lines are the other possible paths found with lower utilities after 15000 iterations. Also, the utilities of all the paths connecting to the possible goal locations are shown in Figures 5.6(b)-5.7(b) with respect to the total length of the paths found.

From these figures, it is seen that the optimization of the proposed utility function leads path search to the least risky areas successfully before the mission completion. Intuitively, avoiding the narrow passages between buildings and flying over wider roads (the traffic activity is omitted in this scenario), yields higher utilities when the impact damage to the properties is considered. However, the behavior of the search can be affected by the conditions in which the UAS operates such as adverse weather conditions, varying vehicle mishap characteristics, etc.

Simulation of normal operating conditions in the first case shows that the expected utility of package delivery to the original goal location is higher. By looking at the path characteristics, it can be inferred that although the shorter alternatives are present, the longer path avoiding the narrow "valleys" until the final approach is found to be better in this case. It is also important to note that the constructed utility function implicitly states that the longer the path is, the higher the chance to have a failure which decreases the final utility of the objective. Therefore, the decision here takes into account the duration of the path as well.

For the second case, increased failure rates push the planner to look for alternatives, which yielded the third location having the higher utility for package delivery among the other locations. However, the utility of delivering the package to the third location is still lower than the utility of the "Do-Not-Fly" action, shown in Figure 5.7(b). This means that flying to deliver a package in the given operating condition is actually less beneficial than staying on the ground. Hence, the decision for the mission should be to not attempt the delivery in this case.

It should be noticed here that the selection of utilities for the mission objectives to construct the desired scenario is not a trivial task and plays a crucial role in the path search and the task-level decisions. For the construction of complex and extensive mission scenarios, more detailed studies are required to establish the relations between utility values and the real-world mission objectives.

CHAPTER 6

CONCLUDING REMARKS AND FUTURE WORK

6.1 Thesis Contribution

In this thesis, a probabilistic risk assessment framework was developed to quantify and assess the risks incurred by the operation of UAS over the populated areas by using the risk exposure modeling of the ground objects and the ground impact modeling of UAS failure modes within the Safe Task-Aware Autonomous Resilient Systems (STAARS) concept. The proposed approach establishes a quantitative method to capture the effects of the factors on the ground safety risk assessment such as the ground exposure characteristics, dynamical vehicle health condition, and environmental inputs. Also, a generic multi-objective optimization approach was introduced to consider both the risk concerns and potential benefits of UAS tasks during the planning and decision-making processes with the purpose of forming a basis for a more holistic decision criterion and task-awareness. Therefore, the proposed framework can be utilized for the path planning of various UAS missions to inform the decision-makers and the planning process as a multi-objective decision and optimization tool by addressing the ground safety concerns and specified mission objectives with their benefits. To illustrate the concept, the minimization of the risks or the maximization of the utilities, which is a blend of risks (negative utility) and benefits (positive utility), along the planned UAS path can be achieved according to the desired considerations. The formulations derived in the concept are generic and flexible enough to cover a wide range of considerations in both risk assessment and the benefit representations, and UAS tasks. As an ultimate goal, this work was intended to be

useful for the development of a regulatory framework for the safe integration of UAS into national airspace by the use of aviation authorities with the complementary and detailed analysis.

6.2 Future Works

The work presented in this thesis can be extended in four potential directions, namely the PREM construction, UAS failure modes and ground impacts, comprehensive risk function and path planning. In the construction of PREM, multiple risk exposure layers corresponding to different risk types and the uncertainty on the modeling of PREM should be incorporated with the current work. Also, the construction of dynamic PREM layers from various data sources such as sensor updates should be demonstrated for real-time applications. In the second direction, a detailed analysis on the UAS failure modes should be performed including the effects of vehicle states and environmental conditions on the ground impact distributions. Another potential extension can be done by improving the risk or cost function used in path planning. In this part, additional factors affecting the cost considerations such as kinetic energy of the platform at the time of impact, the penetration characteristics and the general planning costs including the range and endurance of the operation should be considered. Furthermore, for more realistic analysis and risk considerations, the other ground risk models depicted in Figure 2.3 can be integrated. Lastly, the improvements are required on the path planning algorithm and the implementations for better demonstrations and addressing the realistic scenarios. Some of the improvements can be listed as the incorporation of the vehicle's kinematic and dynamic constraints with a Kinodynamic planner, the path planning in higher dimensions including altitude and more efficient trajectory optimization strategies. To sum up,

although there might be numerous other enhancements in each and every direction, these topics can have major contributions.

REFERENCES

[1] A. Washington, R. A. Clothier, and J. Silva, "A review of unmanned aircraft system ground risk models," *Progress in Aerospace Sciences*, vol. 95, pp. 24 – 44, 2017.

[2] L. C. Barr, R. Newman, E. Ancel, C. M. Belcastro, J. V. Foster, J. Evans, and D. Klyde, "Preliminary risk assessment for small unmanned aircraft systems," 06 2017.

[3] M. Huerta, "Steps being taken to integrate unmanned aircraft systems into the national airspace system." `https://www.transportation.gov/content/steps-being-taken-integrate-unmanned-aircraft-systems-national-airspace-system`, 2015.

[4] E. National Academies of Sciences and Medicine, *Assessing the Risks of Integrating Unmanned Aircraft Systems (UAS) into the National Airspace System*. Washington, DC: The National Academies Press, 2018.

[5] "Deterministic and probabilistic risk." `https://www.preventionweb.net/risk/deterministic-probabilistic-risk`. Accessed: 2019-03-26.

[6] A. M. Dolan and I. Thompson, Richard M., *Integration of Drones into Domestic Airspace: Selected Legal Issues*. 2013.

[7] H. Du and M. A. Heldeweg, "Responsible design of drones and drone services - a synthetic report," 2017.

[8] L. Arona, J. Dale, S. G. Heaslip, M. O. Hammill, and D. W. Johnston, "Assessing the disturbance potential of small unoccupied aircraft systems (uas) on gray seals (halichoerus grypus) at breeding colonies in nova scotia, canada," *PeerJ.*, vol. 6.

[9] F. Christiansen, L. Rojano-Doate, P. T. Madsen, and L. Bejder, "Noise levels of multi-rotor unmanned aerial vehicles with implications for potential underwater impacts on marine mammals," *Frontiers in Marine Science*, vol. 3, p. 277, 2016.

[10] M. J. Logan and L. J. Glaab, "Failure mode effects analysis and flight testing for small unmanned aerial systems," AIAA AVIATION Forum, American Institute of Aeronautics and Astronautics, Jun 2017.

[11] C. M. Belcastro, R. Newman, J. Evans, D. Klyde, L. C. Barr, and E. Ancel, "Hazards identification and analysis for unmanned aircraft system operations," 06 2017.

[12] C. Lum, K. Gauksheim, C. Deseure, J. Vagners, and T. McGeer, "Assessing and estimating risk of operating unmanned aerial systems in populated areas," in *11th AIAA Aviation Technology, Integration, and Operations (ATIO) Conference*, Sep 2011.

[13] J. A. Ball, M. Knott, and D. Burke, "Crash lethality model," Tech. Rep. ADB382358, NAVAL AIR WARFARE CENTER AIRCRAFT DIV PATUXENT RIVER MD, June 2012.

[14] A. la Cour-Harbo, "Ground impact probability distribution for small unmanned aircraft in ballistic descent," 06 2017.

[15] R. Melnyk, *A Framework for Analyzing Unmanned Aircraft System Integration into the National Airspace System Using a Target Level of Safety Approach*. PhD thesis, 05 2013.

[16] N. E. Klepeis *et al.*, "The national human activity pattern survey (nhaps): a resource for assessing exposure to environmental pollutants," *Journal of exposure analysis and environmental epidemiology*, vol. 11, pp. 231–52, 06 2001. Last updated - 2013-01-28.

[17] R. Clothier and R. A Walker, *The Safety Risk Management of Unmanned Aircraft Systems*. 01 2014.

[18] E. Ancel, F. M. Capristan, J. V. Foster, and R. C. Condotta, "Real-time risk assessment framework for unmanned aircraft system (uas) traffic management (utm)," 06 2017.

[19] J. Domercant, O. Pinon, N. C. Knisely, and D. Mavris, "An evaluation framework for unmanned aircraft systems integration in the national airspace system," 06 2014.

[20] G. D. Rito and F. Schettini, "Impacts of safety on the design of light remotely-piloted helicopter flight control systems," *Reliability Engineering and System Safety*, vol. 149, pp. 121–129, 2016.

[21] P. Victerpaul, S. Devaraj, J. Subbiah, and P. Jayabala, "Path planning of autonomous mobile robots: A survey and comparison," *Journal of Advanced Research in Dynamical and Control Systems*, vol. 9, 01 2017.

[22] M. Elbanhawi and M. Simic, "Sampling-based robot motion planning: A review," *IEEE Access*, vol. 2, pp. 56–77, 2014.

[23] S. Karaman and E. Frazzoli, "Incremental sampling-based algorithms for optimal motion planning," *CoRR*, vol. abs/1005.0416, 2010.

[24] M. Jordan and A. Perez, "Optimal bidirectional rapidly-exploring random trees," 08 2013.

[25] C. Wong, E. Yang, X.-T. Yan, and D. Gu, "Optimal path planning based on a multi-tree t-rrt* approach for robotic task planning in continuous cost spaces," pp. 242–247, 09 2018.

[26] S. M. LaValle and J. James J. Kuffner, "Randomized kinodynamic planning," *The International Journal of Robotics Research*, vol. 20, no. 5, pp. 378–400, 2001.

[27] S. M. Lavalle, "Rapidly-exploring random trees: A new tool for path planning," tech. rep., 1998.

[28] S. Karaman and E. Frazzoli, "Sampling-based algorithms for optimal motion planning," *The International Journal of Robotics Research*, vol. 30, no. 7, pp. 846–894, 2011.

[29] D. Devaurs, T. Simon, and J. Corts, "A multi-tree extension of the transition-based rrt: Application to ordering-and-pathfinding problems in continuous cost spaces," in *2014 IEEE/RSJ International Conference on Intelligent Robots and Systems*, pp. 2991–2996, Sep. 2014.

[30] U. C. Kaya, A. Dogan, and M. Huber, "A probabilistic risk assessment framework for the path planning of safe task-aware UAS operations," in *AIAA Scitech 2019 Forum*, American Institute of Aeronautics and Astronautics, Jan 2019.

[31] Microsoft, "Computer generated building footprints for the united states." `https://github.com/Microsoft/USBuildingFootprints`, 2018.

[32] J. Rubio-Hervas, A. Gupta, and Y.-S. Ong, "Data-driven risk assessment and multicriteria optimization of uav operations," *Aerospace Science and Technology*, vol. 77, pp. 510 – 523, 2018.

[33] G. Glonek, T. Staniford, M. Rumsewicz, O. Mazonka, J. McMahon, D. Fletcher, and M. Jokic, "Range safety application of kernel density estimation," Tech. Rep. DSTO-TR-2292, DEFENCE SCIENCE AND TECHNOLOGY ORGANISATION EDINBURGH (AUSTRALIA) WEAPONS SYSTEMS DIV, January 2010.

[34] A. Dogan, "Probabilistic approach in path planning for uavs," in *Proceedings of the 2003 IEEE International Symposium on Intelligent Control*, pp. 608–613, Oct 2003.

[35] R. Aalmoes, Y. S. Cheung, E. Sunil, J. M. Hoekstra, and F. Bussink, "A conceptual third party risk model for personal and unmanned aerial vehicles," in *2015 International Conference on Unmanned Aircraft Systems (ICUAS)*, pp. 1301–1309, June 2015.

[36] F. Grimsley, "Equivalent safety analysis using casualty expectation approach," in *AIAA 3rd "Unmanned Unlimited" Technical Conference, Workshop and Exhibit, Infotech@Aerospace Conferences*, 09 2004.

[37] J. Lazatin, "A method for risk estimation analysis for unmanned aerial system operation over populated areas," in *AIAA AVIATION 2014 -14th AIAA Aviation Technology, Integration, and Operations Conference*, 06 2014.

[38] R. Clothier, R. Walker, N. Fulton, and D. Campbell, "A casualty risk analysis for unmanned aerial system (uas) operations over inhabited areas," 2007.

[39] G. L. Dillingham, *Unmanned Aircraft Systems: Measuring Progress and Addressing Potential Privacy Concerns Would Facilitate Integration into the National Airspace System [Reissued on September 18, 2012]*. 2012.

[40] K. Dalamagkidis, K. P. Valavanis, and L. A. Piegl, "Evaluating the risk of unmanned aircraft ground impacts," in *2008 16th Mediterranean Conference on Control and Automation*, pp. 709–716, June 2008.

BIOGRAPHICAL STATEMENT

Uluhan C. Kaya was born in Kayseri, Turkey, in 1992. He received his Bachelor of Science degree from the Middle East Technical University, Turkey, in 2015 in Aerospace Engineering. In his B.S. degree, he worked on aircraft design, building RC model aircraft and development of control systems in several projects. In Fall 2016, he joined the University of Texas at Arlington to pursue his Master of Science degree in Aerospace Engineering.

He is currently working as a Research Assistant in the Autonomous Vehicle Systems Lab (AVL) with Dr. Manfred Huber, Dr. Atilla Dogan and Dr. Brian Huff on the development of a framework for the safe integration of UAS into National Airspace. He had taken an active role in the Unmanned Vehicle Systems Development courses in UTA as a Teaching Assistant. His research interests consist of simulation, modeling and the advance control methods for the dynamical systems, particularly aircraft systems and autonomous platforms. His work also extends to path/motion planning and intelligent learning algorithms in Robotics field.